The Stability and Dynamics of Hot-Spot Solutions for Two One-Dimensional Microwave Heating Models

David Iron*, Michael J. Ward†

Abstract

The stability and dynamics of hot-spot solutions to two different classes of scalar, nonlocal, singularly perturbed reaction-diffusion equations is analyzed. These problems arise in the modeling of the microwave heating of a ceramic material placed in a single-mode resonant cavity. For the first model, where the coefficients in the differential operator are spatially homogeneous, an explicit characterization of metastable hot-spot behavior is given in the limit of small thermal diffusivity ε. For the second model, where the differential operator has a spatially inhomogeneous term resulting from the variation in the electric field along the ceramic sample, a hot-spot solution is shown to propagate on an algebraically long time-scale of order $O(\varepsilon^{-2})$ towards the point of maximum field strength. The electrical conductivity of the sample is taken to have either an exponential or a polynomial dependence on the temperature. For the polynomial form, the stability of a hot-spot profile is determined from the eigenvalues of a non-self-adjoint eigenvalue problem. It is proved that a general class of eigenvalue problems of this type may have complex conjugate eigenvalues in the limit $\varepsilon \to 0$. A careful proof of the stability of the hot-spot profile is given for this delicate case.

1 Introduction

In this paper we extend the analysis in [4], [5], [6], [17], and [18], on the stability and dynamics of hot-spot solutions that occur for certain singularly perturbed nonlocal reaction-diffusion models. These models arise in the modeling of the microwave heating of ceramics. Nonlocal reaction-diffusion equations also occur in a variety of other areas, such as the Ohmic heating of thermistors (cf. [19]), the propagation of pulses in the singularly perturbed Gray-Scott model (cf. [9], [10]), and the dynamics of spikes in the singularly perturbed Gierer-Meinhardt activator-inhibitor model of morphogenesis (cf. [14], [15]).

*Korteweg-de Vries Instituut, Universiteit van Amsterdam, Amsterdam, Netherlands
†Department of Mathematics, University of British Columbia, Vancouver, Canada V6T 1Z2 (corresponding author)

As shown in [17] and [18], when a thin cylindrical ceramic sample is placed in a resonant single-mode microwave cavity, the temperature of the sample can become very nonuniform. For certain ranges of the parameters, a localized region where the temperature is very large can occur along the axis of the sample (cf. [17], [18]). This localized region of elevated temperature is called a hot-spot. The physical mechanism for the formation of these hot-spots has been modeled for two different physical experiments in [17] and [18].

The analysis in [17] is concerned with placing a thin cylindrical ceramic sample into a cavity resonator in such a way that the intensity of the electric field is constant along the axis of the cylinder. In this case, it was shown in [17] that the mechanism for the formation of a stable hot-spot is the detuning of the cavity that occurs as a result of a large increase in the electrical conductivity of the sample for high temperatures. Depending on the parameters, this detuning shifts the resonant point of the cavity, which reduces the strength of the electric field, and thereby stabilizes the temperature profile. In the small Biot number limit, and for a thin sample, the modeling of this detuning effect leads to a nonlocal reaction-diffusion equation for the dimensionless temperature $u(x,t)$ along the axis of the sample of the form (cf. [17])

$$u_t = \varepsilon^2 u_{xx} - 2\left(u + b[(u+1)^4 - 1]\right) + \frac{p_c f(u)}{1 + \chi^2\left[\int_{-1}^{1} f(u)\,dx\right]^2}\,, \quad |x| \le 1\,; \qquad u_x(\pm 1, t) = 0\,. \quad (1.1)$$

Here ε^2 is the constant thermal diffusivity, $\chi > 0$ is a parameter based on the geometry of the cylinder and the Q-factor of the cavity (see [17]), $b \ll 1$ is the ratio of radiative to convective heat loss along the axis of the sample at the ambient temperature, and $p_c > 0$ is the nondimensional power of the resonant cavity mode. The function $f(u)$ is the dimensionless electrical conductivity of the sample.

The analysis in [18] is based on rotating the thin ceramic sample in the cavity resonator so that the electric field has a spatial variation along the axis of the cylinder. This physical set-up is advantageous for controlling the location of the maximum of the temperature field so that two different cylindrical ceramic materials can be joined together reliably. The analysis in [18], which again incorporates the temperature saturation effect as a result of cavity detuning, has shown that the dimensionless temperature $u(x,t)$ along the axis of the sample satisfies

$$u_t = \varepsilon^2 u_{xx} - 2\left(u + b[(u+1)^4 - 1]\right) + \frac{p_c g(x) f(u)}{(1 + \chi\int_{-1}^{1} g(x) f(u)\,dx)^2}\,, \quad |x| \le 1\,; \qquad u_x(\pm 1, t) = 0\,. \quad (1.2a)$$

Here $g(x)$ is proportional to the square of the dimensionless electric field, and is given by

$$g(x) = \cos^2\left(\frac{\pi}{2}x\right) . \tag{1.2b}$$

In the earlier model of [3] of microwave heating induced hot-spots, the electric field was assumed to be known along the axis of the cylinder, and cavity detuning effects were neglected ($\chi = 0$ in (1.1) and (1.2)). For this reduced model, the existence of a stable hot-spot was due exclusively to an Arrhenius-type model for the electrical conductivity $f(u)$. This model ensured that $f(u)$ is bounded as $u \to \infty$. As discussed in [17] and [18], for ceramic materials below their melting point, the appropriate choice of $f(u)$ based on physical experiments is not an Arrhenius function but, instead, is the exponential form $f(u) = e^{c_1 u}$ for some constant $c_1 > 0$. In [4] and [5], the simpler form $f(u) = (1 + u^2)$ was used in place of the exponential in (1.1) and (1.2). For an $f(u)$ of this polynomial form, we refer to (1.1) and (1.2) as the model microwave heating problems. Although the qualitative features of the dynamics of the hot-spot solutions are similar for both forms of $f(u)$, a distinct technical advantage of using the polynomial form is that, when $\varepsilon \ll 1$, it is much easier to construct asymptotically the homoclinic orbit representing the hot-spot profile. We will consider both forms of $f(u)$

$$f(u) = e^{c_1 u} \quad \text{(experimental)}\,; \qquad f(u) = 1 + u^2 \quad \text{(model)}\,. \tag{1.3}$$

As a remark, any polynomial of the form $f(u) = 1 + c_1 u^p$, for some $c_1 > 0$ and $p > 1$, could also be readily used in the analysis.

For the first model (1.1), it was proved in [4] that, for $\varepsilon \ll 1$ and $f(u) = e^{c_1 u}$, the principal eigenvalue associated with the linearization of (1.1) around an equilibrium hot-spot solution has the asymptotic estimate $\lambda_0 = O(e^{-c/\varepsilon})$ for some $c > 0$. However, a precise estimate for λ_0 was not obtained. A numerical illustration of metastable hot-spot behavior was also given in [4]. For the form $f(u) = (1 + u^2)$, a related proof of metastability for (1.1) for $\varepsilon \ll 1$ was given in [6]. We critique this particular analysis below. The model (1.1) is qualitatively similar to the shadow Gierer-Meinhardt activator-inhibitor model analyzed in [14]. As an extension of the analysis of [4] and [6], we give an explicit characterization of the metastable behavior that occurs for (1.1) for the two choices of $f(u)$ in (1.3). Using a similar formal asymptotic approach as in [14], we give an accurate asymptotic approximation of the exponentially small eigenvalue, and we provide an explicit differential equation governing the motion of the center of the hot-spot. When $f(u) = (1+u^2)$ and $\varepsilon \ll 1$, we show that both the estimate for the exponentially small eigenvalue, and the metastable dynamics are, asymptotically, independent of χ and p_c. For this form of $f(u)$, the analytical results

are compared with numerical results, and close agreement is obtained. Metastable phenomena occurs in many other problems. For a survey see [25].

For the second model (1.2), numerical computations of hot-spot solutions for the case $f(u) = e^{c_1 u}$ were given in [18] together with a numerically-based stability analysis of an equilibrium hot-spot solution. For the case $f(u) = (1+u^2)$, the existence and stability of equilibrium hot-spot solutions for (1.2) was analyzed in [5]. As an extension to these works, we use asymptotic analysis to derive a differential equation for the motion of a hot-spot for (1.2) for both forms of $f(u)$ in (1.3). In our analysis, we will allow for an arbitrary function $g(x)$ in (1.2). The analysis shows that the dynamics of the hot-spot will get pinned to the maximum of $g(x)$ on the domain as $t \to \infty$. Thus, for the $g(x)$ as in (1.2b), the presence of the spatially varying electric field leads to a stable, equilibrium, hot-spot at the center of the domain. For this form of $g(x)$, and for both conductivity models, we show a very favorable comparison between the asymptotic and full numerical results for the hot-spot motion. Pinning effects, whereby the dynamics of a localized structure have new equilibria at certain points in the domain that are a consequence of spatial variations in the coefficients of a singularly perturbed differential operator, occur in many different settings. Applications of pinning include the motion of vortices in superconductivity (cf. [7], [20]), and the role of precursor gradients for spike solutions in the Gierer-Meinhardt model (cf. [16], [26]).

We now summarize the approach used in [4], [5], and [6] for proving the stability of equilibrium hot-spot solutions. The linearization of (1.1) and (1.2) around an equilibrium hot-spot solution leads to a nonlocal eigenvalue problem. Therefore, to examine the stability properties, many spectral results were obtained in [4], [5], and [6], extending earlier fundamental work of [12], for the following class of nonlocal eigenvalue problems:

$$\varepsilon^2 \phi_{xx} + (A(x) - \lambda)\,\phi = B(x) \int_{-1}^{1} C(x)\phi \, dx\,, \qquad -1 < x < 1\,, \tag{1.4a}$$

$$\phi_x(-1) = \phi_x(1) = 0\,. \tag{1.4b}$$

This eigenvalue problem is not self-adjoint unless $B(x) = kC(x)$ for some constant k. For $f(u) = e^{c_1 u}$, the corresponding eigenvalue problem for the linearization around an equilibrium hot-spot solution is self-adjoint. Hence, the eigenvalues are real, and stability follows if one can show that $\lambda < 0$. For this exponential form of $f(u)$, such an approach was used in [4] and [18] to show that equilibrium hot-spot solutions for (1.1) and (1.2) are stable for most parameter regimes. Alternatively, for the polynomial form, $f(u) = (1 + u^2)$, the corresponding eigenvalue problem (1.4) is not self-adjoint and one might initially expect complex eigenvalues. However, even in this non-self-adjoint case, it was claimed in [6] that when $A(x)$, $B(x)$, and $C(x)$ are even functions, the

spectrum of (1.4) is always real, and there are no complex eigenvalues. This claim suggests that any unstable eigenvalues of the linearization around an equilibrium hot-spot solution must lie on the positive real axis in the complex plane. For (1.1) and (1.2) with $f(u) = (1 + u^2)$, it was proved in [6] that there are no such real positive eigenvalues and hence stability of a hot-spot solution followed.

By a counter-example we show that Lemma 4.2 of [6] is, in general, false. Specifically, we construct a simple example of an eigenvalue problem of the form (1.4) with even coefficients $A(x)$, $B(x)$, and $C(x)$, that has complex eigenvalues when $\varepsilon = 1$. Hence, the evenness of the coefficients $A(x)$, $B(x)$, and $C(x)$, is not sufficient to rule out complex eigenvalues for (1.4).

We claim that to determine the stability of an equilibrium hot-spot solution in the limit $\varepsilon \to 0$, we must analyze a slightly different class of eigenvalue problems than (1.4). Instead, we must analyze (1.4) when the even coefficients $A(x)$, $B(x)$, and $C(x)$ in (1.4) are replaced by the even ε-dependent coefficients $A(x/\varepsilon)$, $B(x/\varepsilon)$, and $C(x/\varepsilon)$. We refer to the resulting eigenvalue problem as the modified eigenvalue problem. This is clear since, for $\varepsilon \ll 1$, the equilibrium hot-spot solution is localized near $x = 0$ and has the form $u = U_e(x/\varepsilon)$. The linearization of (1.1) and (1.2) around $U_e(x/\varepsilon)$ leads directly to a specific example of this type of (modified) eigenvalue problem. In the limit $\varepsilon \to 0$, and in the non-self-adjoint case, we show that this class of modified eigenvalue problem can have complex conjugate eigenvalues in the unstable right half-plane even when the coefficients $A(x/\varepsilon)$, $B(x/\varepsilon)$, and $C(x/\varepsilon)$ are even functions. We give a rigorous demonstration of this claim for a particular example related to the shadow Gierer-Meinhardt model. For the microwave heating model with a polynomial conductivity model (1.3), we show numerically that complex conjugate eigenvalues can occur, but that they are in the stable left-half plane.

Therefore, for $\varepsilon \ll 1$, the hot-spot stability analysis of [6] and [5] requires modification for the non-self-adjoint case where $f(u) = (1+u^2)$. Although the conclusion of [6] that the hot-spot solution is stable is correct, we must provide a different analysis to prove stability for this polynomial form of $f(u)$. Our spectral approach can be used to analyze the stability of hot-spot solutions for any polynomial conductivity model of the form $f(u) = 1 + c_1 u^p$, where $c_1 > 0$ and $p > 1$, since the stability of such solutions requires the analysis of non-self-adjoint eigenvalue problems. For the exponential form $f(u) = e^{c_1 u}$, the stability analyses of [4] and [18], which are based on self-adjoint nonlocal eigenvalue problems, are valid for any $\varepsilon > 0$.

The outline of this paper is as follows. In §2 we give a counter-example to show that (1.4) can have a complex conjugate pair of eigenvalues in the unstable right half-plane when $\varepsilon = 1$ and when the even functions $A(x)$, $B(x)$ and $C(x)$ in (1.4) are suitably chosen. We then analyze a class of nonlocal eigenvalue problems of the form (1.4) where the coefficients $A(x)$, $B(x)$, $C(x)$, are replaced

by certain ε-dependent coefficients $A\,(x/\varepsilon)$, $B\,(x/\varepsilon)$, and $C\,(x/\varepsilon)$. In §3, we extend the analysis of [4] to give an explicit characterization of a metastable hot-spot solution for (1.1) when $f(u) = (1+u^2)$ and $\varepsilon \ll 1$. The stability of the hot-spot profile is proved by a different method than in [6]. In §4, we analyze the dynamics of a hot-spot solution for (1.2) when $f(u) = (1+u^2)$ and $\varepsilon \ll 1$, and we prove that the hot-spot profile is stable. In §5, we give an explicit characterization of hot-spot dynamics for (1.1) and (1.2) for the exponential form $f(u) = e^{c_1 u}$. Finally, in §6 we mention a few interesting possible extensions of the analysis of hot-spot solutions to the multi-dimensional case.

2 Complex Eigenvalues of a Nonlocal Eigenvalue Problem

In this section we study a certain eigenvalue problem of the form (1.4). In addition, we analyze a specific generalized form of (1.4) whereby the coefficients $A(x)$, $B(x)$, and $C(x)$, in the differential operator in (1.4) are replaced with ε-dependent coefficients $A(x/\varepsilon)$, $B(x/\varepsilon)$, and $C(x/\varepsilon)$.

2.1 A Counter-Example

We first construct a counter-example to Lemma 4.2 of [6] that asserts that the eigenvalues of (1.4) are real whenever the coefficients $A(x)$, $B(x)$, and $C(x)$ in (1.4a) are even functions. We introduce a continuation parameter δ, with $\delta > 0$, in (1.4). The resulting problem is written in the form

$$\varepsilon^2 \phi_{xx} + (A(x) - \lambda)\,\phi = \delta B(x) \int_{-1}^{1} C(x)\phi\, dx\,, \qquad -1 < x < 1\,, \tag{2.1a}$$

$$\phi_x(-1) = \phi_x(1) = 0\,. \tag{2.1b}$$

To construct our counter-example, we take $\varepsilon = 1$ and choose the even functions $A(x) \equiv 0$, and

$$B(x) \equiv b_0 + b_1 \cos(\pi x) + b_2 \cos(2\pi x)\,, \tag{2.2a}$$

$$C(x) \equiv c_0 + c_1 \cos(\pi x) + c_2 \cos(2\pi x)\,, \tag{2.2b}$$

where the coefficients b_i and c_i, for $i = 0, 1, 2$, are to be chosen.

A simple calculation shows that the eigenfunctions $\psi_k(x)$ and the eigenvalues σ_k of the local operator in (2.1), obtained by setting $\delta = 0$, are

$$\psi_k(x) = \cos\left(\frac{k\pi(x+1)}{2}\right)\,, \qquad \sigma_k = -k^2\pi^2/4\,, \qquad k = 0, 1, 2, 3, \ldots\,. \tag{2.3}$$

These eigenfunctions can be decomposed in terms of even and odd functions as

$$\psi_{2m}(x) = \cos(\pi m x) \ , \qquad \psi_{2m+1}(x) = \sin\left(\frac{(2m+1)\pi x}{2}\right) \ , \qquad m = 0, 1, 2, \ldots . \tag{2.4}$$

The idea of expanding $B(x)$ and $C(x)$ in a subset of the eigenfunctions of the local operator is motivated by [13].

With this choice of $C(x)$, and from (2.1), it is clear from orthogonality that $\lambda = \sigma_k$ and $\phi = \psi_k(x)$ is an eigenpair for (2.1) for any $\delta \geq 0$ and integer $k = 1, 3, 5, 6, 7, \ldots$. These eigenvalues, which are independent of δ and are not perturbed by the nonlocal term, are called the fixed eigenvalues (cf. [12]). The moveable eigenvalues, corresponding to $k = 0, 2, 4$, are perturbed by the nonlocal term and they depend on the continuation parameter δ.

Therefore, the moveable eigenvalues are contained in a three-dimensional subspace of the spectrum of (2.1). In this subspace, we look for an eigenfunction of the form

$$\phi = s_0 + s_1 \cos(\pi x) + s_2 \cos(2\pi x) \ . \tag{2.5}$$

Substituting (2.2) and (2.5) into (2.1), we obtain the 3×3 matrix eigenvalue problem

$$(\Lambda - \delta D)\, \boldsymbol{s} = \lambda \boldsymbol{s} \, , \tag{2.6}$$

where

$$\Lambda \equiv \begin{pmatrix} 0 & 0 & 0 \\ 0 & -\pi^2 & 0 \\ 0 & 0 & -4\pi^2 \end{pmatrix} , \qquad D \equiv \begin{pmatrix} 2c_0 b_0 & c_1 b_0 & c_2 b_0 \\ 2c_0 b_1 & c_1 b_1 & c_2 b_1 \\ 2c_0 b_2 & c_1 b_2 & c_2 b_2 \end{pmatrix} , \qquad \boldsymbol{s} \equiv \begin{pmatrix} s_0 \\ s_1 \\ s_2 \end{pmatrix} . \tag{2.7}$$

The eigenvalues of (2.6) are the moveable eigenvalues of (2.1)

For the special case where $c_i = \kappa b_i$ for $i = 0, 1, 2$, where κ is some constant, the nonlocal Sturm-Liouville eigenvalue problem (2.1) and the matrix eigenvalue problem (2.6) are both self-adjoint. Hence, for this special case, λ is real. However, for arbitrary b_i and c_i, D is a matrix of rank one and $\Lambda - \delta D$ is not a symmetric matrix. Hence, we expect that (2.6) can have complex eigenvalues.

To show this, we choose the coefficients

$$b_0 = 2.5, \quad b_1 = 1.0, \quad b_2 = 1.0 \, , \quad c_0 = 1.1 \, , \quad c_1 = -0.5 \, , \quad c_2 = 0.5 \, . \tag{2.8}$$

With this choice, $B(x)$ and $C(x)$ are positive even functions on $-1 \leq x \leq 1$. We then solve the matrix eigenvalue problem (2.6) numerically as a function of δ. The numerical results are shown in Fig. 1(a) and Fig. 1(b). The eigenvalues are found to be real for $0 \leq \delta < 1.076$ and for

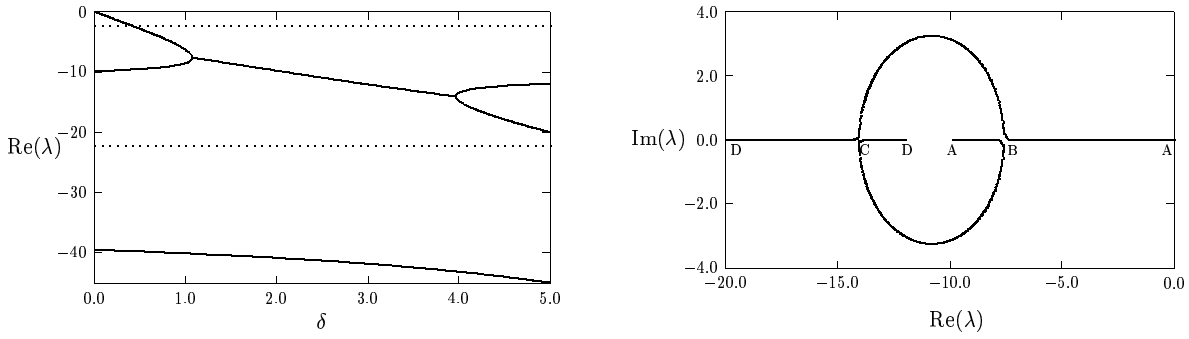

(a) Eigenvalues of (2.6) versus δ

(b) Eigenvalues of (2.6) in the complex plane

Figure 1: Left figure: The real parts of the eigenvalues of (2.6) versus δ for the data (2.8). Two eigenvalues are complex when $1.076 < \delta < 3.970$. The two fixed eigenvalues $\lambda = -\pi^2/4$ and $\lambda = -9\pi^2/4$ are the dotted lines. Right figure: The first two eigenvalues of (2.6) and (2.8) in the complex plane. Points A,B,C, and D, correspond to $\delta = 0.0$, $\delta = 1.076$, $\delta = 3.97$, and $\delta = 5.0$.

$3.970 < \delta < 5.0$. As δ is increased to $\delta = 1.076$ the first and second eigenvalues merge and enter the complex plane. Then, as δ is increased further to $\delta = 3.970$, this complex conjugate pair of eigenvalues merges onto the real axis.

This counter-example clearly shows that the evenness of the coefficients $A(x)$, $B(x)$, and $C(x)$ is not sufficient to ensure that (1.4) will only have real eigenvalues, as was claimed in [6]. The mechanism for the creation of complex eigenvalues as δ increases is that a pair of moveable real eigenvalues collide when traveling in opposite directions (see Fig. 1(b)) and then enter the complex plane. This can occur when a moveable eigenvalue crosses past a fixed eigenvalue as δ increases. In particular, in the example above there are consecutive fixed eigenvalues at $\lambda = -9\pi^2/4$ and $\lambda = -\pi^2/4$. These eigenvalues correspond to the horizontal dotted lines in Fig. 1(a). From this figure we notice that there can be a pair of moveable eigenvalues between consecutive fixed eigenvalues for some range of δ. This mechanism for the creation of complex eigenvalues from the collision of two moveable eigenvalues also occurs for other nonlocal eigenvalue problems, including the more complicated eigenvalue problems of §2.2.

2.2 A Nonlocal Eigenvalue Problem: Stability of a Localized Solution

We now consider a specific class of eigenvalue problem that is related to the linearization of a nonlocal PDE around a localized pulse. This problem can be written in the form

$$\varepsilon^2\phi_{xx} + A\left(x/\varepsilon\right)\phi - B\left(x/\varepsilon\right)\int_{-1}^{1} C\left(x/\varepsilon\right)\phi\, dx = \lambda\phi\,, \qquad |x| \le 1\,; \qquad \phi_x(\pm 1) = 0\,, \tag{2.9}$$

where $A(x/\varepsilon)$, $B(x/\varepsilon)$, and $C(x/\varepsilon)$, are even functions.

To construct our example, we consider the following eigenvalue problem for $\Phi^\varepsilon(y)$:

$$\mathcal{L}_\varepsilon\Phi^\varepsilon \equiv L_\varepsilon\Phi^\varepsilon - \alpha w_\varepsilon^p\left(\frac{\int_{-1/\varepsilon}^{1/\varepsilon} w_\varepsilon^{m-1}\Phi^\varepsilon\, dy}{\int_{-1/\varepsilon}^{1/\varepsilon} w_\varepsilon^m\, dy}\right) = \lambda^\varepsilon\Phi^\varepsilon\,, \qquad |y| \le 1/\varepsilon\,; \qquad \Phi_y^\varepsilon(\pm\varepsilon^{-1}) = 0\,. \tag{2.10}$$

Here $\alpha \ge 0$ is a continuation parameter, and we assume that the exponents p and m are real and satisfy $p > 1$, $m > 1$, and $p \ne m-1$. The operator L_ε, referred to as the local operator, is defined by

$$L_\varepsilon\Phi^\varepsilon \equiv \Phi^\varepsilon_{yy} - \Phi^\varepsilon + pw_\varepsilon^{p-1}\Phi^\varepsilon\,. \tag{2.11}$$

Here $w_\varepsilon(y)$ is the unique one-pulse solution of the boundary value problem

$$w_\varepsilon'' - w_\varepsilon + w_\varepsilon^p = 0\,, \quad |y| \le \varepsilon^{-1}\,; \qquad w_\varepsilon(0) > 0\,, \quad w_\varepsilon'(0) = 0\,; \qquad w_\varepsilon'\left(\pm 1/\varepsilon\right) = 0\,. \tag{2.12}$$

Such a solution is even $w_\varepsilon(y) = w_\varepsilon(-y)$, it has a single maximum at $y = 0$, and satisfies $w_\varepsilon' < 0$ for $0 < y < 1/\varepsilon$.

By writing $y = x/\varepsilon$ in (2.9), it is clear that, for each $\varepsilon > 0$ fixed, (2.10) is a specific example of (2.9). Since $p \ne m-1$, (2.9) is not self-adjoint. This class of eigenvalue problem arises in the study of the stability of spike solutions to the Gierer-Meinhardt model of morphogenesis (see [23] and Appendix C below). As shown below in §3.4, the particular case $p = m$ is the relevant eigenvalue problem for studying the stability of a hot-spot profile for (1.1) for the generalized polynomial conductivity model $f(u) = 1 + c_1 u^p$.

We first study the limiting eigenvalue problem, corresponding to letting $\varepsilon \to 0$ in (2.10) and (2.12) and imposing an exponential decay condition on Φ^ε and w_ε as $y \to \pm\infty$. This limiting eigenvalue problem, which has both a discrete and a continuous spectrum, is referred to below as the infinite-line problem. Using a combination of numerical and rigorous analytical techniques, we show that this infinite-line problem can have complex discrete eigenvalues for some ranges of α, p, and m. This was previously shown numerically for the case $(p, m) = (2, 2)$ in [14] and later in [8]. In §2.3, we give a rigorous proof that the infinite-line problem will have complex conjugate

eigenvalues in the unstable right half-plane for some range of α when $p = 6$ and $m = 2$. Other cases of p and m leading to complex discrete eigenvalues for the infinite-line problem are shown numerically.

The corresponding discrete eigenfunctions in the right half-plane are found to decay exponentially as $|y| \to \infty$. This suggests that, for a small but fixed value of ε, the effect of a large but finite domain in (2.10) and (2.12) will be to perturb these eigenpairs by exponentially small terms as $\varepsilon \to 0$. We illustrate this weak dependence on the length of the domain numerically. Therefore, our main conclusion is that complex eigenvalues are possible for eigenvalue problems of the form (2.9) in the singularly perturbed limit $\varepsilon \to 0$, and that these eigenvalues persist when ε is small but nonzero.

We begin by considering the infinite-line problem. We define the local operator L_0 for this problem by

$$L_0\Phi^0 \equiv \Phi^0_{yy} - \Phi^0 + pw_0^{p-1}\Phi^0\,, \tag{2.13}$$

where w_0 is the unique, even, one-pulse positive solution to (2.12) on $-\infty < y < \infty$. A simple calculation shows that

$$w_0(y) = \left(\frac{p+1}{2}\right)^{1/(p-1)} \left(\cosh\left[\frac{(p-1)y}{2}\right]\right)^{-2/(p-1)}\,. \tag{2.14}$$

The homoclinic orbit $w_0(y)$ has the following asymptotic behavior

$$w_0(y) \sim ce^{-|y|}\,, \qquad |y| \to \infty\,, \qquad c \equiv (2p+2))^{1/(p-1)}\,. \tag{2.15}$$

Therefore, the nonlocal eigenvalue problem on the infinite line is given by

$$\mathcal{L}_0\Phi^0 \equiv L_0\Phi^0 - \alpha w_0^p\left(\frac{\int_{-\infty}^{\infty} w_0^{m-1}\Phi^0\,dy}{\int_{-\infty}^{\infty} w_0^m\,dy}\right) = \lambda\Phi^0\,, \qquad -\infty < y < \infty\,; \qquad \Phi^0 \to 0\,, \quad |y| \to \infty\,. \tag{2.16}$$

We first summarize a few known result for the spectrum of L_0 and of $\mathcal{L}_0$.

Proposition 2.1 (From [21]): *Consider the local eigenvalue problem $L_0\phi_l = \nu\phi_l$ for $\phi_l \in \mathcal{H}^1(R)$. This problem admits the eigenvalues $\nu_0 > 0$, $\nu_1 = 0$, and $\nu_j < 0$ for $j > 1$. The eigenvalue ν_0 is simple, and the corresponding eigenfunction ϕ_{l0} has one sign.*

Thus, there is exactly one unstable eigenvalue $\nu_0 > 0$ for the infinite-line local eigenvalue problem. By solving this problem in terms of certain hypergeometric functions, a more explicit result for the spectrum of L_0 was obtained in [9].

Proposition 2.2 (From [9]): *Let $J = J(p)$ be a positive integer such that $J < (p+1)/(p-1) \leq J+1$. Then, for $\phi_l \in \mathcal{H}^1(R)$, the infinite-line local eigenvalue problem $L_0\phi_l = \nu\phi_l$ has $J+1$ discrete eigenvalues given by*

$$\nu_j = \frac{1}{4}\left[(p+1) - j(p-1)\right]^2 - 1\,, \qquad j = 0, .., J\,. \tag{2.17}$$

The continuous spectrum of L_0 lies in the range $-\infty < \nu < -1$.

This result is Proposition 5.6 of [9]. Notice that $\nu_0 > 0$, $\nu_1 = 0$, and $\nu_j \in (-1, 0)$ for $2 \leq j \leq J$. However, when $p \geq 3$, then $J = 1$, and there are no discrete eigenvalues in the interval $(-1, 0)$.

The following result for the spectrum of $\mathcal{L}_0$ was obtained in [27] and [15]:

Proposition 2.3 (From [27]): *Let $\Phi^0 \in \mathcal{H}^1(R)$, and consider the eigenvalue problem (2.16) with $m = 2$. Consider only the eigenpairs of this problem for which $\lambda \neq 0$. Let $\lambda_0^0 \neq 0$ be the eigenvalue of (2.16) with the largest real part. Then, if $0 \leq \alpha < p-1$, we have $Re(\lambda_0^0) > 0$. Alternatively, if $\alpha > p-1$ and if either of the following two conditions hold*

$$\text{(i)} \quad m = 2\,, \quad 1 < p \leq 5\,, \qquad \text{or} \qquad \text{(ii)} \quad m = p+1\,, \quad p > 1\,,$$

then $Re(\lambda_0^0) < 0$.

The proof of the result for $0 \leq \alpha < p-1$ is given in Appendix E of [15]. The proof of the result for $\alpha > p-1$ is given in Lemma A and Theorem 1.4 of [27]. This result shows that any eigenvalues of (2.16) must lie in the stable left half-plane if α is large enough and if $1 < p \leq 5$.

Next, we numerically compute the spectrum of (2.10) as a function of α for different ranges of p and m. This is done by using a finite difference scheme on (2.10). First we take a value of ε small, which determines the domain length. We then compute a numerical approximation for the solution w_ε to (2.12) using COLSYS [2]. We introduce a uniform mesh with N points, and approximate the second derivative ϕ_{xx} using a central difference quotient. The integral in (2.10) is approximated by the trapezoidal rule. The eigenvalues of the resulting matrix eigenvalue problem are then computed numerically using an eigenvalue solver routine from LAPACK [1]. In all of the computations below we have taken $N = 400$ points. For four pairs (p, m) of exponents, and with $\alpha = 0$, in Table 1 we give the theoretical predictions for the discrete eigenvalues for the infinite-line problem obtained from Proposition 2.2, together with the corresponding numerically computed values from (2.10) with $\varepsilon = 0.05$ and $\varepsilon = 0.20$. The eigenvalues for (2.10) with $\varepsilon = 0.05$ are seen to be close to those for the infinite-line problem.

We remark that the infinite line problem has a double-zero eigenvalue when $\alpha = \alpha_c \equiv p - 1$. This follows from the identity that

$$L_0 w_0 = (p-1) w_0^p\,. \tag{2.19}$$

(p, m)	λ_0 (infinite-line)	λ ($\varepsilon = 0.05$)	λ ($\varepsilon = 0.20$)
(2,2)	1.25000	1.25029	1.24580
	0.00000	0.83032×10^{-3}	0.51828×10^{-4}
	-0.75000	-0.74916	-0.82947
(6,2)	11.2500	11.2835	11.2487
	0.0000	0.31476×10^{-1}	0.19214×10^{-2}
(3,3)	3.0000	3.00190	2.99793
	0.0000	0.368875×10^{-2}	0.22996×10^{-3}
(1.39,1.2)	0.428025	0.428056	0.291304
	0.000000	0.119973×10^{-3}	-0.477610×10^{-2}
	-0.351975	-0.351747	-0.498224
	-0.627900	-0.627609	-1.18901
	-0.827775	-0.827522	-2.07709
	-0.951600	-0.953261	-3.16240
	-0.999375	-1.02567	-4.44489

Table 1: The discrete eigenvalues for the infinite-line problem (2.16) obtained from Proposition 2.2, and the corresponding numerically computed discrete eigenvalues obtained from (2.10) with $\varepsilon = 0.05$ and $\varepsilon = 0.20$.

When $\alpha = \alpha_c$, both $\Phi^0 = w_0$ and $\Phi^0 = w_0'$ are eigenfunctions of (2.16) corresponding to $\lambda = 0$. At this critical value $\alpha = \alpha_c$, and for $\varepsilon = 0.05$ and $\varepsilon = 0.20$, in Table 2 we give numerical results for the eigenvalue of (2.10) that approximates the even eigenfunction $\Phi^0 = w_0$ of the infinite-line problem (2.16). From this table we observe that this eigenvalue is small for both $\varepsilon = 0.05$ and $\varepsilon = 0.20$. Therefore, the finite-line problem (2.10) with $\varepsilon = 0.05$ and $\varepsilon = 0.20$ has two small eigenvalues at the critical value $\alpha = \alpha_c$ for which the infinite-line problem has a double-zero eigenvalue.

(p, m)	λ ($\varepsilon = 0.05$)	λ ($\varepsilon = 0.20$)
(2,2)	0.1747×10^{-3}	0.4367×10^{-2}
(6,2)	-0.2799×10^{-1}	-0.2138×10^{-1}
(3,3)	0.8336×10^{-3}	0.7808×10^{-4}
(1.39,1.2)	0.6393×10^{-4}	-0.1586×10^{-2}

Table 2: The eigenvalue of (2.10) for $\varepsilon = 0.05$ and $\varepsilon = 0.20$, corresponding to an even eigenfunction when $\alpha = \alpha_c \equiv p - 1$. At this value of α, the infinite-line problem (2.16) has a double-zero eigenvalue.

Example 1: Let $p = m = 2$, with $\varepsilon = 0.05$ or $\varepsilon = 0.20$. This was the exponent set first studied

numerically in [14]. When $\alpha = 0$, there are two discrete eigenvalues on the real axis as seen from Proposition 2.2. As seen from Table 1, the numerical values for the eigenvalues of the infinite-line problem and the finite domain problem (2.10) with $\varepsilon = 0.05$ and $\varepsilon = 0.20$ are both very close. As shown in Fig. 2, when $\varepsilon = 0.05$ these two discrete eigenvalues travel in opposite directions as α is increased, and are found to merge at the value $\lambda \approx -.541$ on the negative real axis when $\alpha = 1.31$. Similar behavior occurs when $\varepsilon = 0.20$. In this case, the two discrete eigenvalues collide at $\lambda_R \approx -0.598$ when $\alpha \approx 1.3515$. The results for $\varepsilon = 0.05$ are consistent with the original results in [14] and the later study in [8]. As α is increased further, the complex eigenvalues then tend towards the negative real axis on $\lambda_R \equiv \mathrm{Re}(\lambda) < -1$. The behavior in the left half-plane when $\varepsilon = 0.05$ and $\varepsilon = 0.20$ is found to be rather different, especially when the path approaches the "continuous" spectrum region $\lambda_R < -1$. In particular, the complex conjugate eigenvalues with $\varepsilon = 0.20$ touch down onto the real axis at $\lambda_R \approx -1.12$ when $\alpha \approx 2.23$. The path with $\varepsilon = 0.05$ is more intricate. ■

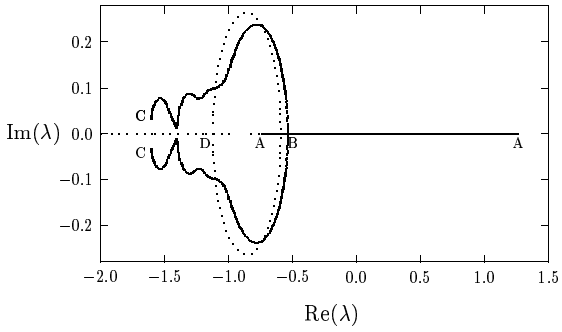

Figure 2: Complex eigenvalues for (2.10) when $(p, m) = (2, 2)$ with $\varepsilon = 0.05$ (heavy solid line) and $\varepsilon = 0.20$ (dotted line). Points A, B, and C, correspond to $\alpha = 0.0$, $\alpha = 1.31$, and $\alpha = 2.5$, when $\varepsilon = 0.05$. Point D corresponds to $\alpha = 2.23$ when $\varepsilon = 0.20$. The "continuous" spectrum region (horizontal dotted line) is the portion $\lambda_R < -1$ of the horizontal axis.

Example 2: Let $p = 6$, $m = 2$, and $\varepsilon = 0.05$, or $\varepsilon = 0.20$. When $\alpha = 0$, Proposition 2.2 shows that there is exactly one discrete eigenvalue on the real axis for the infinite-line problem (2.16). From Table 1 it is closely approximated by the eigenvalue problem (2.10) with $\varepsilon = 0.05$ and $\varepsilon = 0.20$. As α is increased, this eigenvalue moves along the real axis towards the left. As shown in Fig. 3(a) a new discrete eigenvalue emerges out of the "continuous" spectrum region $\lambda_R \equiv \mathrm{Re}(\lambda) < -1$ as

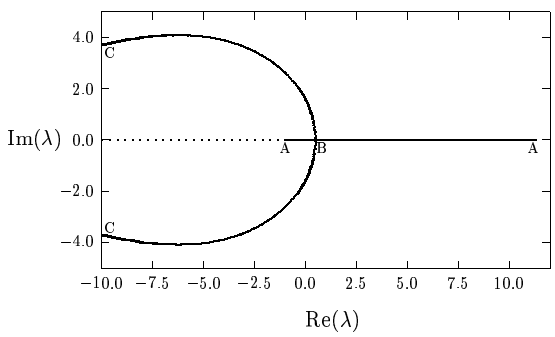

(a) Complex eigenvalues for (2.10) with $(p, m) = (6, 2)$

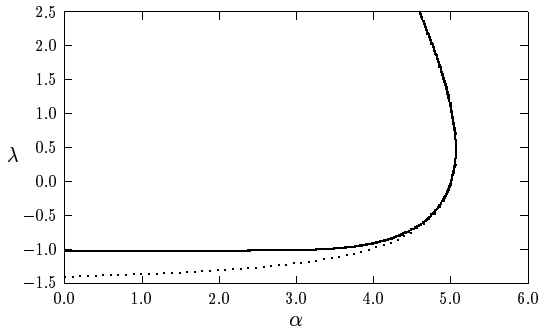

(b) The discrete and edge bifurcation eigenvalues

Figure 3: Left figure: Complex spectra for (2.10) when $(p, m) = (6, 2)$ with $\varepsilon = 0.05$ (heavy solid) and $\varepsilon = 0.20$ (dotted). Points A, B, and C, correspond to $\alpha = 0.0$, $\alpha = 1.31$, and $\alpha = 2.5$, for $\varepsilon = 0.05$. The "continuous" spectrum is the horizontal dotted line. Right figure: Discrete and edge bifurcation eigenvalues of (2.10) before they merge: $\varepsilon = 0.05$ (heavy solid) $\varepsilon = 0.20$ (dotted).

α increases. When $\varepsilon = 0.05$, the two eigenvalues collide on the positive real axis at $\lambda_R \approx 0.477$ when $\alpha \approx 5.05$. When $\varepsilon = 0.20$, the corresponding values are $\lambda_R \approx 0.465$ and $\alpha \approx 5.06$. As shown in Fig. 3(a), after the collision this pair enters the left half-plane as α is increased and eventually the eigenvalue path tends towards the negative real axis. The eigenvalue paths for $\varepsilon = 0.05$ and $\varepsilon = 0.20$ are virtually indistinguishable in Fig. 3(a) on the range $0 \leq \alpha \leq 2.5$. For $\varepsilon = 0.05$ and $\varepsilon = 0.20$, in Fig. 3(b) we plot the edge bifurcation eigenvalue as a function of α up until it collides with the path of the discrete eigenvalue that originated in the right half-plane when $\alpha = 0$. Notice that the path of the edge bifurcation eigenvalue does depend significantly on ε. A rigorous treatment of this problem for eigenvalues in the right half-plane is given in §2.3. ■

Example 3: Let $p = 3$, $m = 3$, with $\varepsilon = 0.05$ or $\varepsilon = 0.20$. As shown in §3.4 below, this eigenvalue problem arises in the study of the stability of a hot-spot profile for the polynomial conductivity model $f(u) = 1 + c_1 u^3$. When $\alpha = 0$, Proposition 2.2 shows that there is exactly one discrete eigenvalue on the real axis for the infinite-line problem. From Table 1 it is again closely approximated by the eigenvalue problem with $\varepsilon = 0.05$. As shown in Fig. 4, as α is increased this eigenvalue moves along the real axis towards the left. However, in contrast to Example 2, there

appears to be no eigenvalue that emerges from the continuous spectrum that will collide with this discrete eigenvalue at some value of α. As α is increased, the path of the discrete eigenvalue is found to lie on the real axis until it merges with the "continuous" spectrum region. In Fig. 4 we plot this eigenvalue as a function of α for both $\varepsilon = 0.05$ and $\varepsilon = 0.20$. The eigenvalue paths for these two values of ε are virtually indistinguishable on this graph. ■

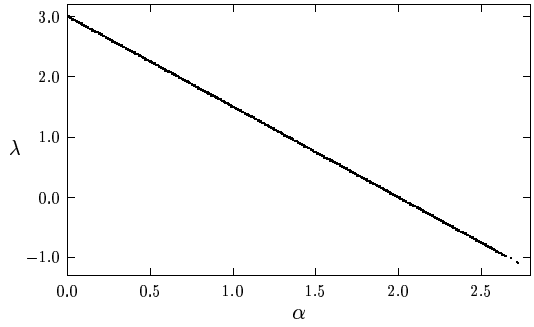

Figure 4: The path of the discrete eigenvalue for (2.10) when $(p, m) = (3, 3)$ as a function of α. This eigenvalue remains real until it merges with the "continuous" spectrum region $\lambda_R \equiv \mathrm{Re}(\lambda) < -1$. The heavy solid curve is for $\varepsilon = 0.05$ and the dotted curve is for $\varepsilon = 0.20$. These curves are indistinguishable here.

Example 4: Next we let $p = 1.39$, $m = 2$, with $\varepsilon = 0.05$ or $\varepsilon = 0.20$. From Proposition 2.2, there are seven discrete eigenvalues for the infinite-line problem (2.16) when $\alpha = 0$. The discrete spectrum is composed of three fixed eigenvalues, which are independent of α, and four moveable eigenvalues, which depend on α. As seen from Table 1, when $\varepsilon = 0.05$ and $\alpha = 0$ all of these eigenvalues, except for the last moveable eigenvalue, are closely approximated by eigenvalues of the finite domain problem (2.10). However, the eigenvalues for (2.16) and (2.10) are considerably different when $\varepsilon = 0.20$ and $\alpha = 0$.

In Fig. 5 we plot the eigenvalues in the complex plane for $\varepsilon = 0.05$ on the range $0 \le \alpha \le 1.5$. From this figure, we observe that there are two separate collisions of moveable eigenvalues on this interval. There is a collision at $\lambda \approx -0.233$ when $\alpha \approx 0.532$ and another at $\lambda \approx -0.99$ when $\alpha \approx 1.36$. In Fig. 6(a) we plot the real parts of these eigenvalues as a function of α (solid curves) together with the first three fixed eigenvalues (dotted curves). Notice that this plot is qualitatively similar to Fig. 1(a) for the counter-example of §2.1. For the larger value $\varepsilon = 0.20$, in Fig. 6(b) we plot the real parts of the first four moveable eigenvalues together with the first three fixed

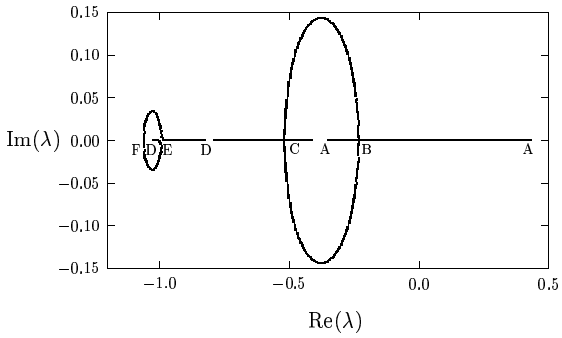

Figure 5: Complex eigenvalues for (2.10) when $(p, m) = (1.39, 1.2)$ with $\varepsilon = 0.05$ (heavy solid curves) on the range $0 < \alpha < 1.5$. There are two collisions of moveable eigenvalues producing complex spectra. Points A, B, C, D, E, and F, correspond to $\alpha = 0.0$, $\alpha = 0.532$, $\alpha = 1.11$, $\alpha = 0$, $\alpha = 1.36$, and $\alpha = 1.50$.

eigenvalues. For this case, no collisions of moveable eigenvalues occur for $0 \leq \alpha \leq 1.5$. ■

Finally, we comment on the dependence of the eigenvalues on the domain length $2/\varepsilon$. In Table 1 we showed numerically that, when $\alpha = 0$, the discrete eigenvalues of the infinite-line problem (2.16) are closely approximated by those of the finite line problem (2.10) when $\varepsilon = 0.05$. When $\varepsilon = 0.20$, the agreeement is again close except for the exponent set $(p, m) = (1.39, 1.2)$. For the exponent sets $(p, m) = (6, 2)$ (Example 2) and $(p, m) = (3, 3)$ (Example 3), the paths of the discrete eigenvalues as a function of α were virtually identical for both $\varepsilon = 0.20$ and $\varepsilon = 0.05$. For these two values of ε, qualitatively similar behavior was obtained for the case $(p, m) = (2, 2)$, except near the "continuous" spectrum region. For the exponent set $(p, m) = (1.39, 1.2)$, the spectral behavior with $\varepsilon = 0.05$ and $\varepsilon = 0.20$ was significantly different.

To qualitatively explain these differences, in Fig. 7(a) and Fig. 7(b) we plot the numerical solution w_ε to (2.12) for $\varepsilon = 0.05$ and $\varepsilon = 0.20$, respectively. The plots are shown for Examples 1–4, where $p = 6$, $p = 3$, $p = 2$, and $p = 1.39$. Notice that w_ε is more localized for higher values of p. Therefore, at a fixed value of ε, the effect of the finite domain is more significant for lower values of p. For the infinite-line problem, the corresponding solution w_0 decays exponentially. However, Fig. 7(a) and Fig. 7(b) suggest that w_ε does not closely approximate w_0 for small values of p unless ε is very small.

We conjecture that the discrete eigevalues of the infinite-line problem (2.16) and the finite-line problem (2.10) should be close as $\varepsilon \to 0$ whenever both w_ε and the eigenfunction of the infinite-line

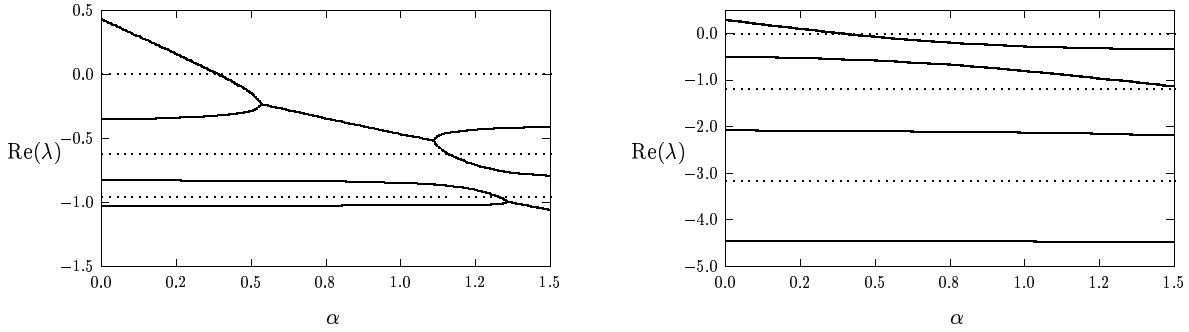

(a) Real parts of the eigenvalues: $\varepsilon = 0.05$

(b) Real parts of the eigenvalues: $\varepsilon = 0.20$

Figure 6: Left figure: Real parts of the eigenvalues of (2.10) when $(p, m) = (1.39, 1.2)$ with $\varepsilon = 0.05$. The first four moveable eigenvalues are the heavy solid curves and the dotted curves are the first three fixed eigenvalues. Right figure: Same plot as in the left figure except that $\varepsilon = 0.20$.

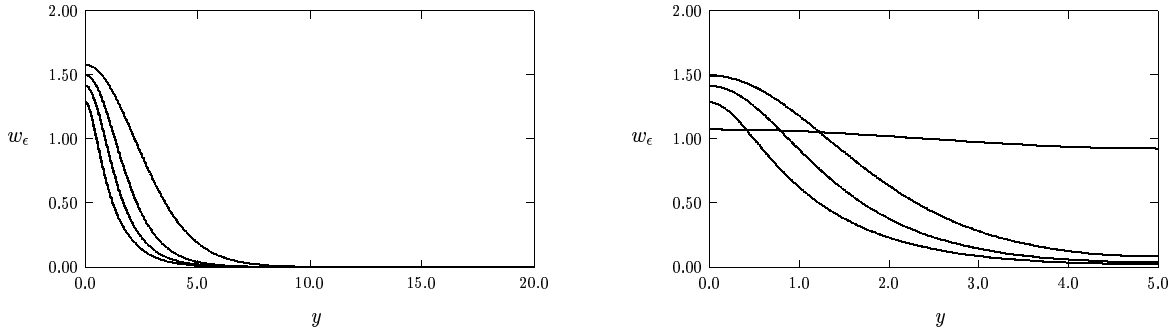

(a) w_ε for $\varepsilon = 0.05$

(b) w_ε for $\varepsilon = 0.20$

Figure 7: Left figure: Numerical solution to (2.12) for $p = 6$, $p = 3$, $p = 2$, and $p = 1.39$ when $\varepsilon = 0.05$. Higher to lower values of p correspond to lower to higher values of $w_\varepsilon(0)$. Right figure: Same plot except for $\varepsilon = 0.20$.

problem are exponentially small at the endpoints $y = \pm\varepsilon^{-1}$ for the finite domain problem. As $\varepsilon \to 0$, w_ε is always exponentially small at $y = \pm\varepsilon^{-1}$, but the behavior is nonuniform in p. The infinite-line eigenfunction will only decay exponentially as $|y| \to \infty$ provided that the corresponding eigenvalues are bounded away from the continuous spectrum region. Therefore, for $\varepsilon \to 0$, the behavior near the continuous spectrum region should depend sensitively on ε. However, the spectra of (2.10) and (2.16) in the right half-plane should be close when ε is sufficiently small, since both the eigenfunction of the infinite-line problem and w_ε are exponentially small at the endpoints $y = \pm\varepsilon^{-1}$. For a fixed ε small, the finite domain problem will provide a poorer approximation to the spectrum of the infinite-line problem as p decreases, since then w_ε becomes less localized.

A rigorous treatment of the effect of ε is difficult. A first step in this direction was made in [8], where the effect of the finite domain was analyzed rigorously for the local eigenvalue problem (2.10) obtained by setting $\alpha = 0$. In [8], it was proved that the first three eigenvalues of this problem satisfy

$$\lambda_0 = \frac{1}{4}(p-1)(p+3) + O\left(e^{-2/\varepsilon}\right), \tag{2.20a}$$

$$\lambda_1 = O\left(e^{-2/\varepsilon}\right), \tag{2.20b}$$

$$\lambda_2 = \frac{1}{4}(p-1)(p-5) + O\left(e^{-(3-p)/\varepsilon}\right), \qquad \text{when} \quad p < 3\,. \tag{2.20c}$$

It would be interesting to try to extend these error estimates to the nonlocal eigenvalue problem where $\alpha > 0$.

2.3 Unstable Complex Eigenvalues: Nonlocal Problem on Infinite Line

The behavior of the spectrum when $p > 5$, and for certain ranges of m, is not covered by Proposition 2.3. In this section we will consider the case $m = 2$ and $p > 5$. The numerical computations of §2.2 suggest that for this choice of exponents, (2.16) will have complex conjugate eigenvalues in the unstable right half-plane for a certain range of α. To prove this, we will examine the spectrum of (2.16) with $m = 2$ on both the real and the imaginary axis. We then use a winding number approach to count the number of eigenvalues of (2.16) in the unstable right half-plane.

It is convenient to reformulate (2.16) when $m = 2$ into a form more amenable to analysis. Let $\psi(y)$ be the solution to

$$L_0\psi \equiv \psi'' - \psi + pw_0^{p-1}\psi = \lambda\psi + w_0^p\,; \qquad \psi \to 0 \quad \text{as} \quad |y| \to \infty\,. \tag{2.21}$$

Therefore, when $m = 2$, the eigenfunctions of (2.16) can be written as

$$\Phi^0 = \alpha \left(\frac{\int_{-\infty}^{\infty} w_0 \Phi^0 \, dy}{\int_{-\infty}^{\infty} w_0^2 \, dy} \right) \psi \,. \tag{2.22}$$

We then multiply both sides of (2.22) by w_0 and integrate over the domain. We assume that $\int_{-\infty}^{\infty} w_0 \Phi^0 \, dy \neq 0$. Thus, in the reformulated problem, the zero eigenvalue with corresponding eigenfunction $w_0'(y)$ is conveniently eliminated. We then obtain a transcendental relation for the eigenvalues of (2.16) given by the roots of $g(\lambda) = 0$, where

$$g(\lambda) \equiv \frac{1}{\alpha} - f(\lambda) \,, \qquad f(\lambda) \equiv \frac{\int_{-\infty}^{\infty} w_0 \psi \, dy}{\int_{-\infty}^{\infty} w_0^2 \, dy} \,, \qquad (L_0 - \lambda)\, \psi = w_0^p \,. \tag{2.23}$$

We begin by separating (2.23) into real and imaginary parts by writing

$$g = g_R + i g_I \,, \qquad f = f_R + i f_I \,, \qquad \lambda = \lambda_R + i \lambda_I \,, \qquad \psi = \psi_R + i \psi_I \,. \tag{2.24}$$

Substituting (2.24) into (2.23), we obtain

$$g_R(\lambda) = \frac{1}{\alpha} - f_R(\lambda) \,, \qquad f_R(\lambda) \equiv \frac{\int_{-\infty}^{\infty} w_0 \psi_R \, dy}{\int_{-\infty}^{\infty} w_0^2 \, dy} \,, \tag{2.25a}$$

$$g_I(\lambda) = -f_I(\lambda) \,, \qquad f_I(\lambda) \equiv \frac{\int_{-\infty}^{\infty} w_0 \psi_I \, dy}{\int_{-\infty}^{\infty} w_0^2 \, dy} \,. \tag{2.25b}$$

In (2.25), the functions ψ_R and ψ_I, obtained from separating real and imaginary parts in (2.23), satisfy the coupled system

$$L_0 \psi_R = \lambda_R \psi_R - \lambda_I \psi_I + w_0^p \,; \qquad L_0 \psi_I = \lambda_R \psi_I + \lambda_I \psi_R \,, \tag{2.26}$$

with $\psi_R \to 0$ and $\psi_I \to 0$ as $|y| \to \infty$.

We first look for a pure imaginary eigenvalue of the form $\lambda = i\lambda_I$. Without loss of generality we may assume that $\lambda_I > 0$. From (2.25) and (2.26), the eigenvalues of (2.16) along the positive imaginary axis $\lambda_I > 0$ are the roots of the coupled system $\tilde{g}_R = \tilde{g}_I = 0$, given by

$$\tilde{g}_R(\lambda_I) \equiv \frac{1}{\alpha} - \tilde{f}_R(\lambda_I) \,, \qquad \tilde{g}_I(\lambda_I) \equiv -\tilde{f}_I(\lambda_I) \,, \tag{2.27a}$$

where

$$\tilde{f}_R(\lambda_I) \equiv \frac{\int_{-\infty}^{\infty} w_0 L_0 \left[L_0^2 + \lambda_I^2 \right]^{-1} w_0^p \, dy}{\int_{-\infty}^{\infty} w_0^2 \, dy} \,, \qquad \tilde{f}_I(\lambda_I) \equiv \frac{\lambda_I \int_{-\infty}^{\infty} w_0 \left[L_0^2 + \lambda_I^2 \right]^{-1} w_0^p \, dy}{\int_{-\infty}^{\infty} w_0^2 \, dy} \,. \tag{2.27b}$$

In the analysis below, we need a few properties of the functions $\tilde{f}_R$ and $\tilde{f}_I$. These properties are summarized as follows:

Proposition 2.4: *The functions $\tilde{f}_R$ and $\tilde{f}_I$ in (2.27b) have the asymptotic behavior*

$$\tilde{f}_R(\lambda_I) \sim \frac{1}{p-1} - \kappa_c \lambda_I^2 + O(\lambda_I^4), \quad \text{as} \quad \lambda_I \to 0; \qquad \tilde{f}_R(\lambda_I) = 0\left(\lambda_I^{-2}\right), \quad \text{as} \quad \lambda_I \to \infty, \tag{2.28a}$$

$$\tilde{f}_I(\lambda_I) \sim \frac{\lambda_I}{p-1}\left[\frac{1}{p-1} - \frac{1}{4}\right] + O(\lambda_I^3), \quad \text{as} \quad \lambda_I \to 0; \quad \tilde{f}_I(\lambda_I) = \frac{c_0}{\lambda_I} + O\left(\lambda_I^{-3}\right), \quad \text{as} \quad \lambda_I \to \infty, \tag{2.28b}$$

where

$$\kappa_c \equiv \frac{1}{(p-1)} \frac{\int_{-\infty}^{\infty} \left[L_0^{-1} w_0\right]^2 dy}{\int_{-\infty}^{\infty} w_0^2 \, dy} > 0, \qquad c_0 \equiv \frac{\int_{-\infty}^{\infty} w_0^{p+1} dy}{\int_{-\infty}^{\infty} w_0^2 \, dy} > 0. \tag{2.28c}$$

For $p > 1$, the following global result holds for $\tilde{f}_R'$

$$\tilde{f}_R'(\lambda_I) < 0, \quad \text{for} \quad \lambda_I > 0. \tag{2.28d}$$

For $1 < p \leq 5$, the following global result hold for $\tilde{f}_I$

$$\tilde{f}_I(\lambda_I) > 0, \quad \text{for} \quad \lambda_I > 0. \tag{2.28e}$$

The proof of these results are given in Propositions 3.1 and 3.2 of [23]. For the convenience of the reader, we outline the key steps in Appendix A.

From (2.28e) and (2.27a), we conclude that $\tilde{g}_I < 0$ for $\lambda_I > 0$ when $1 < p \leq 5$. Hence, for $1 < p \leq 5$, there are no eigenvalues of (2.16) on the imaginary axis. However, suppose that $p > 5$. Then, from the local behavior (2.28b) for $\tilde{f}_I$ near $\lambda_I = 0$ we conclude that $\tilde{f}_I < 0$ on some interval including the origin. In addition, from (2.28b) we have that $\tilde{f}_I > 0$ for $\lambda_I \gg 1$ with $\tilde{f}_I \to 0^+$ as $\lambda_I \to \infty$. Hence, there must be a root λ_I^0 to $\tilde{g}_I = 0$ in (2.27a). Setting $\tilde{g}_R = 0$ in (2.27a), we obtain a critical value for α, labeled by α_h, given by

$$\alpha_h = \left[\tilde{f}_R(\lambda_I^0)\right]^{-1}. \tag{2.29}$$

Since $\tilde{f}_R$ is monotone decreasing for $\lambda_I > 0$ and $\tilde{f}_R(0) = 1/(p-1)$, we have that $\alpha_h > p - 1$. Thus, for $p > 5$, there will be a pair of complex conjugate eigenvalues on the imaginary axis when $\alpha = \alpha_h$. We are unable to prove that $\tilde{g}_I = 0$ has a unique root. However, this detail is immaterial for proving the existence of this complex conjugate pair of eigenvalues.

We now give some numerical results for $p = 6$. We first use COLSYS to solve (2.26) for ψ_R and ψ_I for each value of $\lambda_I > 0$. We find numerically that $\tilde{g}_I = 0$ has exactly one root. Newton's method is used to locate the value $\lambda_I = \lambda_I^0$ for which $\tilde{g}_I = 0$. We then calculate α_h from (2.29). In this way, we obtain numerically that

$$\alpha_h = 5.5318\,, \qquad \lambda_I^0 = 1.5296\,, \qquad \text{when} \quad p = 6\,. \tag{2.30}$$

These values compare well with the numerical results obtained from the finite difference computations of §2.2. In the numerically computed figures, Fig. 8(a) and Fig. 8(b), we show the graphical determination of the root of $\tilde{g}_R = \tilde{g}_I = 0$. In Fig. 8(b) we plot $\tilde{f}_I$ versus λ_I. There is indeed one root to $\tilde{g}_I = 0$ at λ_I^0. We remark that $\tilde{f}_I$ is monotone decreasing for $\lambda_I \geq 13$, which is beyond the range of the plot. In Fig. 8(a), we plot $\tilde{f}_R$ and $1/\alpha_h$. These curves intersect at λ_I^0. In this figure, we also plot two other values of α.

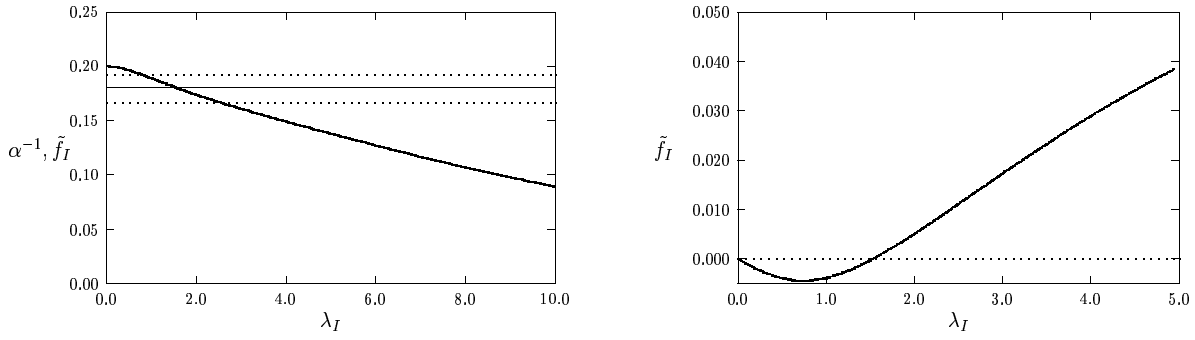

(a) $\tilde{g}_R = 0$: plots of $\tilde{f}_R$ and $1/\alpha$

(b) $\tilde{g}_I = 0$: plots of $\tilde{f}_I$

Figure 8: The roots of $\tilde{g}_R = \tilde{g}_I = 0$ shown graphically for $p = 6$. The heavy solid curves in the left and right figures are $\tilde{f}_R$ and $\tilde{f}_I$, respectively. The solid curve in the left figure is $1/\alpha_h$, which intersects $\tilde{f}_R$ at the root of $\tilde{f}_I = 0$. The top and bottom dashed curves in the left figure are $1/\alpha$ for $\alpha = 5.2$ and $\alpha = 6.0$, respectively.

To determine the number of eigenvalues in the unstable right-half plane as a function of α, we use a winding number approach. We calculate the winding number of $g(\lambda)$ in (2.23) over the counterclockwise contour composed of the imaginary axis $-iR \leq \mathrm{Im}\lambda \leq iR$ and the semi-circle Γ_R, given by $|\lambda| = R > 0$, for $-\pi/2 \leq \arg\lambda \leq \pi/2$. Assuming that α is chosen so that there are no

zeros of $g(\lambda)$ on the imaginary axis, we let $R \to \infty$ and use the argument principle to determine the number of zeros of $g(\lambda)$ in the right half-plane. The function $g(\lambda)$ in (2.23) is analytic in the right half-plane, except at the simple pole $\lambda = \nu_0 > 0$, where ν_0 is the unique positive eigenvalue of the local operator L_0 (see Propositions 2.1 and 2.2 above). From (2.23), it follows that there is a constant C, with C independent of λ, for which $f(\lambda) \sim C/\lambda$ on Γ_R, when $R \equiv |\lambda| \gg 1$. Hence, for $R \gg 1$, $g(\lambda) \sim \alpha^{-1}(1 - \alpha C/\lambda)$. From this asymptotic formula it follows that the change in the argument of g over Γ_R as $R \to \infty$ is 0. Hence, by using the argument principle, the number of eigenvalues M of (2.16) in the right half-plane $\mathrm{Re}(\lambda) > 0$ when $m = 2$ is

$$M = 1 + \frac{1}{\pi}\left[\arg g\right]_{\Gamma_I} . \tag{2.31}$$

Here $[\arg g]_{\Gamma_I}$ denotes the change in the argument of g along the semi-infinite imaginary axis $\Gamma_I = i\lambda_I$, $0 \le \lambda_I < \infty$, traversed in the downwards direction. This leads to the next proposition.

Proposition 2.5 *Let $p > 5$, and assume that that $(p-1) < \alpha < \alpha_h$. Then, there are exactly two eigenvalues in the right half-plane. When $0 < \alpha < (p-1)$ and $p > 5$, there is exactly one eigenvalue in the right half-plane.*

The proof is simple. We need only calculate $[\arg g]_{\Gamma_I}$ in (2.31). However, since we do not have a uniqueness proof for the root of $\tilde{g}_I = 0$, we will take α_h to correspond to the smallest root λ_I^0 of $\tilde{g}_I = 0$. Hence, by the local behavior (2.28b), we have $\tilde{g}_I > 0$ on the interval $(0, \lambda_I^0)$. For $\alpha > 0$, we have from Proposition 2.4 that $\tilde{g}_R \to 1/\alpha > 0$ and $\tilde{g}_I \to 0$ as $\lambda_I \to \infty$. Hence, the starting point for the argument of g on Γ_I is on the positive real axis in the $\tilde{g}_R$, $\tilde{g}_I$ plane. At $\lambda_I = 0$, we have from (2.28a), and the condition on α in Proposition 2.5, that $\tilde{f}_R(0) = 1/(p-1) > 1/\alpha$ and $\tilde{f}_I(0) = 0$. Thus, the ending point for the argument of g is on the negative real axis in the $\tilde{g}_R$, $\tilde{g}_I$ plane. Next, the monotonicity result (2.28d) proves that for each α, with $\alpha > (p-1)$, the equation $\tilde{g}_R = 0$ is satisfied at only one value of λ_I. The sign of $\tilde{g}_I$ at this unique root of $\tilde{g}_R = 0$ determines whether the winding number is π or $-\pi$. For $(p-1) < \alpha < \alpha_h$, we will have $\tilde{g}_I > 0$ at the unique root of $\tilde{g}_R = 0$ (see Fig. 8(a) where we illustrate this graphically). Hence, $[\arg g]_{\Gamma_I} = \pi$, and from (2.31) we get $M = 2$. When $0 \le \alpha < p-1$, we have $\tilde{g}_R > 0$ for all $\lambda_I > 0$. Thus, $[\arg g]_{\Gamma_I} = 0$, and from (2.31) we get $M = 1$. This completes the proof of Proposition 2.5. This result also shows a transversality condition, in that when $p > 5$ and for each α in the range $(p-1) < \alpha < \alpha_h$, there will be exactly two eigenvalues in the right half-plane $\mathrm{Re}(\lambda) > 0$.

Next, we analyze the spectrum of (2.16) when $m = 2$ on the real axis $\lambda = \lambda_R$. On the real axis, (2.23) is written as

$$g(\lambda) = g_R(\lambda_R) \equiv \frac{1}{\alpha} - f_R(\lambda_R)\,, \qquad f_R(\lambda_R) = \frac{\int_{-\infty}^{\infty} w_0 \left(L_0 - \lambda_R\right)^{-1} w_0^p \, dy}{\int_{-\infty}^{\infty} w_0^2 \, dy}\,. \tag{2.32}$$

Since L_0 has one positive real eigenvalue, the function $f_R(\lambda_R)$ is analytic for $\lambda_R > 0$ except at the point $\lambda_R = \nu_0$, where $\nu_0 > 0$ is the principal eigenvalue of the local operator L_0. As $\lambda_R \to \nu_0^-$, we have $f_R(\lambda_R) \to +\infty$. Further properties of the behavior of $f_R(\lambda_R)$ are obtained in [23], and are summarized as follows.

Proposition 2.6: *Let $p > 1$ and ν_0 be the principal eigenvalue of the local operator L_0. The function f_R in (2.32) has the asymptotic behavior*

$$f_R(\lambda_R) \sim \frac{1}{p-1} + \frac{\lambda_R}{p-1}\left[\frac{1}{p-1} - \frac{1}{4}\right] + \kappa_c \lambda_R^2 + O(\lambda_R^3)\,, \quad \text{as} \quad \lambda_R \to 0\,, \tag{2.33a}$$

with $f_R \to +\infty$ as $\lambda_R \to \nu_0^-$. Here κ_c is given in (2.28c). For $1 < p \leq 5$, we have the global result,

$$f_R'(\lambda_R) > 0\,, \quad \text{for} \quad 0 < \lambda_R < \nu_0\,. \tag{2.33b}$$

Finally, on the interval $\lambda_R > \nu_0$, we have

$$f_R(\lambda_R) < 0\,, \quad \text{for} \quad \lambda_R > \nu_0\,. \tag{2.33c}$$

For the convenience of the reader we outline the key steps in the derivation of this result in Appendix B. When $1 < p \leq 5$, equation (2.33b), and the fact that $f_R(0) = 1/(p-1)$ proves that there is exactly one root λ_R^0 of $g_R(\lambda_R) = 0$ on the interval $0 < \lambda_R < \nu_0$ for any α with $0 < \alpha < p-1$. For $1 < p \leq 5$, $\lambda_R^0 \to \nu_0^-$ as $\alpha \to 0^+$, and $\lambda_R^0 = 0$ when $\alpha = p - 1$. Thus, when $1 < p \leq 5$ and $m = 2$, (2.16) has no complex eigenvalues in the right half-plane. Moreover, when $1 < p < 5$ and $0 \leq \alpha < p - 1$, there is only one unstable eigenvalue and it is on the positive real axis.

Now suppose that $p > 5$. The global result (2.33c) shows that any roots of $g_R = 0$ must be in the interval $0 \leq \lambda_R < \nu_0$ when $\alpha > 0$. Then, the local behavior (2.33a) proves that $f_R'(0) < 0$, and so f_R is locally decreasing for $\lambda_R > 0$. However, from Proposition 2.5, where we have counted the number of eigenvalues in the right half-plane precisely, it follows that the horizontal line $1/\alpha$ can only intersect f_R exactly once when $0 < \alpha < (p-1)$. It can intersect f_R at most twice for $\alpha > (p-1)$. Thus, the function $f_R(\lambda_R)$ can have only one minimum at some value $\lambda_R = \lambda_R^0$, and the corresponding minimum value of f_R must be less that $1/(p-1)$. At this minimum point, $g_R = 0$ has a double root. Let α_m correspond to the value of α for which $g_R = 0$ has a double root. Then, for $0 < \lambda_R < \nu_0$, we have

$$\alpha_m^{-1} = \text{Min}\,[f_R(\lambda_R)]\,. \tag{2.34}$$

This is the critical value of α where the complex conjugate pair of eigenvalues merge onto the real axis. When $p = 6$, we calculate numerically that

$$\alpha_m = 5.0521\,, \qquad \lambda_R^0 = 0.4662\,. \tag{2.35}$$

Thus, on the range $(p-1) < \alpha < \alpha_m$, we have two eigenvalues on the positive real axis. When $\alpha_m < \alpha < \alpha_h$, there is a complex conjugate pair of eigenvalues in the unstable right half-plane. For $0 \leq \alpha < (p-1)$, there is one eigenvalue on the positive real axis. Hence, one real eigenvalue crosses into the left half-plane as α is decreased below $(p-1)$.

We summarize our main result of this section as follows:

Proposition 2.7: *Let $\Phi \in \mathcal{H}^1(R)$, $m = 2$, and suppose that $p > 5$ in (2.16). Then, for any $\alpha > 0$ there are at most two eigenvalues in the unstable right half-plane $Re(\lambda) > 0$. For $0 < \alpha < p-1$, there is one eigenvalue in the right half-plane. This eigenvalue is real and is on the interval $(0, \nu_0)$. For $(p-1) < \alpha < \alpha_m$, there are exactly two eigenvalues on the positive real axis in the interval $(0, \nu_0)$. At the value $\alpha = \alpha_m$, these real eigenvalues coalesce. For $\alpha_m < \alpha < \alpha_h$, there is a pair of complex conjugate eigenvalues in the unstable right half-plane $Re(\lambda) > 0$. When $\alpha = \alpha_h$, there are a pair of complex conjugate eigenvalues on the imaginary axis.*

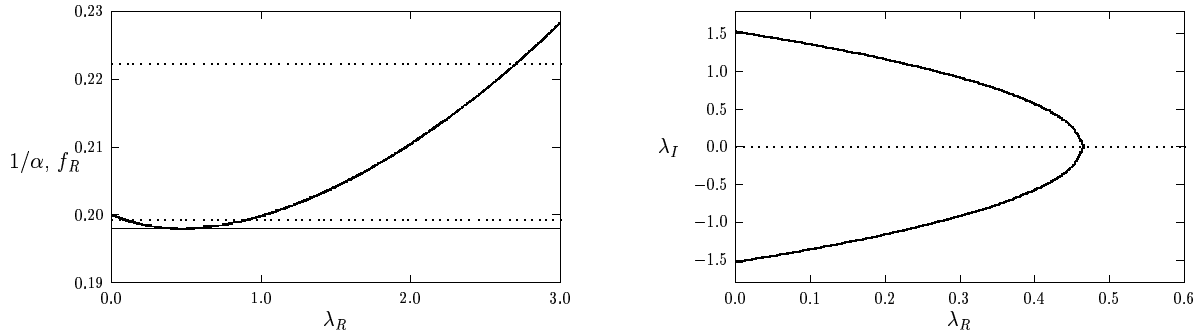

(a) $g_R = 0$: plots of f_R and $1/\alpha$ (b) $\lambda = \lambda_R \pm i\lambda_I$

Figure 9: Left figure: Plots of f_R (heavy solid curve) and $1/\alpha_m$ (solid curve). The top and bottom dashed curves is $1/\alpha$ with $\alpha = 4.5$ and $\alpha = 5.02$, respectively. When $\alpha = 4.5$ there is one root to $g_R = 0$. There are two roots when $\alpha = 5.02$. Right figure: Plot of the path $\lambda = \lambda_R \pm i\lambda_I$ as α decreases below $\alpha_h = 5.5318$. The paths converge onto the real axis at $\alpha = \alpha_m = 5.0521$ with $\lambda_R = 0.4662$.

Finally, we illustrate our results for the case $p = 6$. In Fig. 9(a) we show the graphical determination of the roots of $\tilde{g}_R = 0$. In Fig. 9(b) we plot the numerically computed path for the complex conjugate eigenvalues on the range $\alpha_m < \alpha < \alpha_h$. These results were computed by using COLSYS

to solve (2.26) and Newton's method to compute the roots to $g(\lambda) = 0$.

As a remark, suppose that $p > 5$, $m = 2$, with $\alpha > 0$ and $\alpha \ll 1$. Then, (2.16) has one eigenvalue on the positive real axis. Recall that for $p \geq 3$, Proposition 2.2 proves that there are no eigenvalues in the left half-plane on the interval $-1 < \lambda_R < 0$ when $\alpha = 0$. However, as α is increased above $(p-1)$, an eigenvalue of (2.16) crosses through the origin along the real axis into the unstable right half-plane as was shown numerically in §2.2. This eigenvalue presumably arises from an edge bifurcation off of the continuous spectrum located on $\lambda_R < -1$. Such a crossing occurs not just for the exponents $p > 5$ and $m = 2$, but it occurs for other values of p and m. To see this, we look for the zeros of (2.32) along the real axis, where $f_R(\lambda_R)$ in (2.32) is replaced by

$$f_R(\lambda_R) = \frac{\int_{-\infty}^{\infty} w_0^{m-1} \left(L_0 - \lambda_R\right)^{-1} w_0^p \, dy}{\int_{-\infty}^{\infty} w_0^m \, dy} \, . \tag{2.36}$$

The local behavior of $f_R(\lambda_R)$ near λ_R was calculated in [23], where the following result, analogous to (2.33a), was obtained

$$f_R(\lambda_R) \sim \frac{1}{p-1} + \frac{\lambda_R}{p-1}\left[\frac{1}{p-1} - \frac{1}{2m}\right] + O\left(\lambda_R^2\right) \, . \tag{2.37}$$

Thus, $f_R(\lambda_R)$ is locally decreasing near $\lambda_R = 0$ when $p - 1 > 2m$. In addition, we have $f_R \to +\infty$ as $\lambda_R \to \nu_0^-$. Hence, we conclude that when $p - 1 > 2m$, then $g(\lambda_R) = 0$ in (2.32) has at least two roots on $0 < \lambda_R < \nu_0$ for α in the range $p - 1 < \alpha < \alpha_c$, for some α_c. Therefore, when $p - 1 > 2m$, there are at least two real eigenvalues along the positive real axis for some range of α. Since $m > 1$, this can only occur when $p - 1 > 2m > 2$, so that $p > 3$. Notice, however, that when $p > 3$, Proposition 2.3 proves that there is only one discrete eigenvalue when $\alpha = 0$, and it is along the positive real axis. Therefore, we conjecture that when $p - 1 > 2m$ and $m > 1$, this extra eigenvalue that crosses into the right half-plane along the real axis arises from an edge bifurcation off of the continuous spectrum associated with the infinite-line problem. The numerical results obtained from Examples 2 and 3 in §2.2, showed that there was no edge bifurcation for the exponent set $(p, m) = (3, 3)$, but that one occurred when $(p, m) = (6, 2)$. Similar edge bifurcations are common occurrences in the study of dispersive waves. This mechanism of an edge bifurcation suggests the subtlety required for the analysis of singularly perturbed eigenvalue problems.

In conclusion, the example in this section has given a rigorous proof that the evenness of the functions $A(x/\varepsilon)$, $B(x/\varepsilon)$, and $C(x/\varepsilon)$, in the non-self-adjoint problem (2.9) is insufficient to guarantee that (2.9) will have only real eigenvalues in the limit $\varepsilon \to 0$.

3 Metastability for the Model Problem

In this section we analyze the stability and dynamics of a hot-spot solution for (1.1) in the limit $\varepsilon \to 0$ when $f(u) = (1+u^2)$. We write (1.1) as

$$u_t = \varepsilon^2 u_{xx} - 2\left(u + b[(u+1)^4 - 1]\right) + \frac{p_c(1+u^2)}{(1+\chi^2 I^2)}\,, \quad |x| \le 1\,; \qquad u_x(\pm 1, t) = 0\,, \tag{3.1a}$$

where I is defined by

$$I \equiv \int_{-1}^{1} (1+u^2)\, dx\,. \tag{3.1b}$$

We assume that $p_c > 0$ and $\chi > 0$ are $O(1)$ as $\varepsilon \to 0$.

The transient formation of a hot-spot from an initial condition $u(x,0)$, representing a small spatial variation of a constant initial state, is described qualitatively in [17] for the exponential conductivity model $f(u) = e^{c_1 u}$. The discussion in [17] also applies to the polynomial form of $f(u)$ given above. Our analysis in this section is complementary to that given in [17], in that we describe the long-term behavior of a hot-spot solution after it has formed from initial data.

We first determine a scaling so that $u = O(1)$ as $\varepsilon \to 0$ at the center of a hot-spot. Since $u \to \infty$ as $\varepsilon \to 0$ in the hot-spot region (cf. [17], [6]), we introduce the new variable $U(x,t)$ by $u = \varepsilon^{-a} U$, for some $a > 0$. Then, the dominant terms in (3.1) for $\varepsilon \ll 1$ are

$$U_t = \varepsilon^2 U_{xx} - 2\left(U + b\varepsilon^{-3a} U^4\right) + \frac{p_c \varepsilon^{-a} U^2}{(1+\chi^2 \varepsilon^{2-4a} I_\varepsilon^2)}\,, \quad |x| \le 1\,; \qquad U_x(\pm 1, t) = 0\,, \tag{3.2a}$$

where

$$I = \varepsilon^{1-2a} I_\varepsilon\,, \qquad I_\varepsilon \equiv \varepsilon^{-1} \int_{-1}^{1} U^2\, dx\,. \tag{3.2b}$$

If U is localized near some point in the domain on a length-scale of $O(\varepsilon)$, then $I_\varepsilon = O(1)$ as $\varepsilon \to 0$. To balance the terms in (3.2a) we take $a = 2/3$. In [4] and [5], b is taken to be small. We will assume that $b \ll O(\varepsilon^2)$. Then, from (3.2), we obtain the re-scaled problem

$$U_t = \varepsilon^2 U_{xx} - 2U + \frac{p_c U^2}{\chi^2 I_\varepsilon^2}\,, \quad |x| \le 1\,; \qquad U_x(\pm 1, t) = 0\,, \tag{3.3a}$$

where

$$I = \varepsilon^{-1/3} I_\varepsilon\,, \qquad I_\varepsilon \equiv \varepsilon^{-1} \int_{-1}^{1} U^2\, dx\,. \tag{3.3b}$$

Although our scaling is based on a balance of terms to ensure that $U = O(1)$ as $\varepsilon \to 0$ in the hot-spot region, (3.3) is also a uniformly valid approximation of (3.1) across the entire domain when $b \ll \varepsilon^2$. To see this, suppose that the hot-spot is located at $x = x_0$. Then, away from this region, $u \sim u_c$, where u_c is the spatially homogeneous outer solution. From (3.1), u_c satisfies the algebraic equation

$$2\left(u_c + b[(u_c+1)^4 - 1]\right) = \frac{p_c(1+u_c^2)}{(1+\chi^2 I^2)}\,. \tag{3.4}$$

Here I is defined in (3.1b). In an $O(\varepsilon)$ region defining the core of the hot-spot we have shown that $u = O(\varepsilon^{-2/3})$, and consequently $I = O(\varepsilon^{-1/3})$ as given in (3.3b). With $I = O(\varepsilon^{-1/3})$ in (3.4), we obtain that $u_c = O(\varepsilon^{2/3})$ for $\varepsilon \ll 1$. Hence, we may use (3.3) for U, with $U \to 0$ away from the hot-spot region, as a uniformly valid leading order approximation to the solution u to (3.1). However, we do need to assume that $b \ll \varepsilon^2$, so that the u^4 term in (3.1a) is small even in the hot-spot region.

Next, we construct the hot-spot profile using matched asymptotic expansions. To do so, we introduce the inner variables v and y for the hot-spot region, defined by

$$y = \varepsilon^{-1}(x - x_0)\,, \qquad v(y,t) = U(x_0 + \varepsilon y, t)\,. \tag{3.5}$$

Here the hot-spot location x_0 is taken to be any point in $-1 < x_0 < 1$. Then, the spatial profile of the hot-spot is obtained by substituting (3.5) into the steady-state version of (3.3). This yields that v satisfies

$$v_{yy} - 2v + \frac{p_c v^2}{\chi^2 I_0^2} = 0\,; \qquad -\infty < y < \infty\,, \qquad I_0 \equiv \int_{-\infty}^{\infty} v^2\,dy\,, \tag{3.6}$$

with $v \to 0$ as $|y| \to \infty$. To solve (3.6) we write $v(y) = \gamma w(\zeta y)$, for some γ and ζ to be chosen. Here $w(\xi)$ is the unique positive solution to

$$w'' - w + w^2 = 0\,, \quad -\infty < \xi < \infty\,; \quad w(0) > 0\,, \quad w'(0) = 0\,; \quad w \to 0 \quad \text{as} \quad |\xi| \to \infty\,. \tag{3.7}$$

We calculate that

$$I_0 = \gamma^2 \zeta^{-1} \int_{-\infty}^{\infty} w^2\,d\xi\,, \qquad \gamma = \frac{p_c^{1/3}}{\chi^{2/3}\left(\int_{-\infty}^{\infty} w^2\,d\xi\right)^{2/3}}\,, \qquad \zeta = \sqrt{2}\,. \tag{3.8}$$

This leads to the following proposition:

Proposition 3.1: *For $\varepsilon \to 0$, the hot-spot profile $U_\varepsilon = U_\varepsilon[x;x_0]$ is given by*

$$U \sim U_\varepsilon[x;x_0] \equiv \gamma w\left[\sqrt{2}\varepsilon^{-1}(x-x_0)\right]\,, \qquad \gamma \equiv \left(\frac{p_c}{36\chi^2}\right)^{1/3}\,. \tag{3.9a}$$

Here $w(\xi)$ is the solution to (3.7). The solution to (3.7) is

$$w(\xi) = \frac{3}{2}\mathrm{sech}^2\,(\xi/2)\;, \qquad \text{with} \qquad \int_{-\infty}^{\infty} [w(\xi)]^2\; d\xi = 6\,. \tag{3.9b}$$

For $\varepsilon \to 0$, the nonlocal term I in (3.3b) is

$$I \sim \varepsilon^{-1/3} I_0\,, \qquad I_0 = 3\sqrt{2}\left(\frac{p_c}{36\chi^2}\right)^{2/3}\,. \tag{3.10}$$

A plot of a typical profile for U_ε is shown in Fig. 10. A similar result was obtained in [6] using a dynamical systems approach.

Notice that the function U_ε satisfies the steady-state problem for (3.3a) exactly, but it fails to satisfy the boundary conditions in (3.3a) by only exponentially small terms as $\varepsilon \to 0$ for any x_0 in the interval $-1 < x_0 < 1$. This near translation invariance is the first indication that metastable dynamics can occur in (1.1). By symmetry, under the Neumann boundary conditions, the equilibrium hot-spot location must be at the origin $x_0 = 0$.

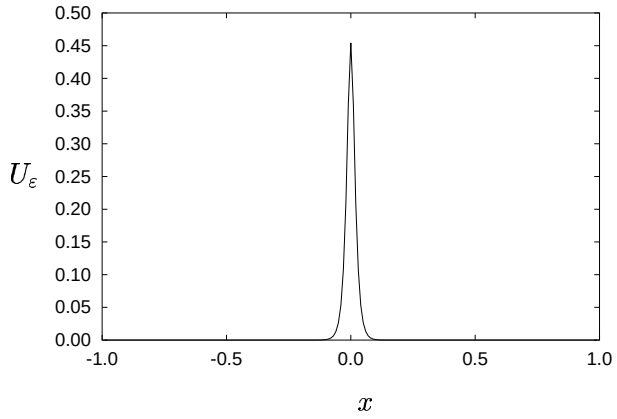

Figure 10: Plot of the equilibrium hot-spot solution U_ε to (3.3) with $x_0 = 0$, $\varepsilon = 0.01$, $p_c = \chi = 1.0$.

3.1 The Eigenvalue Problem: Stability of The Profile

In this section we examine the stability of the hot-spot profile. With U_ε as defined in Proposition 3.1, we let

$$u(x,t) = U_\varepsilon + e^{\lambda t}\phi\,. \tag{3.11}$$

Substituting (3.11) into (3.3), and linearizing, we obtain the eigenvalue problem for ϕ,

$$L_\varepsilon \phi \equiv \varepsilon^2 \phi_{xx} + \left(-2 + \frac{2p_c U_\varepsilon}{\chi^2 I_0^2} \right) \phi - \frac{4p_c U_\varepsilon^2}{\varepsilon \chi^2 I_0^3} \int_{-1}^{1} U_\varepsilon \phi \, dx = \lambda \phi \,, \quad |x| \le 1 \,, \tag{3.12a}$$

$$\phi_x(\pm 1) = 0 \,. \tag{3.12b}$$

Since U_ε is localized near x_0, this eigenvalue problem has the form as given in (2.9), with even ε-dependent coefficients $A(x/\varepsilon)$, $B(x/\varepsilon)$, and $C(x/\varepsilon)$. Therefore, since this problem can have complex eigenvalues, as was discussed in §2, we must prove stability in a different way than in [6].

We now show that in the limit $\varepsilon \to 0$, and for any $\chi > 0$ and $p_c > 0$, (3.12) does not have any eigenvalue with $\mathrm{Re}(\lambda_0) > 0$. To do so, we use an approach similar to that in §2. For $\varepsilon \to 0$, we look for a localized eigenfunction $\phi = \Phi(\xi)$ of (3.12), where $\xi \equiv \sqrt{2}\varepsilon^{-1}(x - x_0)$. Then, using the formulae for U_ε and I_0 in Proposition 3.1, (3.12) can be written in a form similar to (2.16) with $p = m = 2$. After a little algebra, we obtain

$$\Phi_{\xi\xi} - \Phi + 2w\Phi - \alpha w^2 \left(\frac{\int_{-\infty}^{\infty} w\Phi \, d\xi}{\int_{-\infty}^{\infty} w^2 \, d\xi} \right) = \frac{\lambda}{2} \Phi \,, \qquad -\infty < \xi < \infty \,, \tag{3.13a}$$

where $\Phi \to 0$ as $|\xi| \to \infty$, and $w(\xi)$ is the solution to (3.7). The constant α in (3.13a) is

$$\alpha \equiv \frac{6\sqrt{2}\, p_c \gamma^3}{\chi^2 I_0^3} \,, \tag{3.13b}$$

where γ is defined in (3.9a). Therefore, (3.13) has exactly the same form as (2.16) when $p = m = 2$ in (2.16). Therefore, Proposition 2.3, due to [27], gives a necessary and sufficient condition for the stability of the profile U_ε. From Proposition 2.3, we conclude that there are no eigenvalues of (3.13) with $\mathrm{Re}(\lambda) > 0$, if and only if $\alpha > 1$ in (3.13b). A simple calculation using the expressions for γ and I_0 in (3.9a) and (3.10), respectively, yields that $\alpha = 4$ for all $\chi > 0$ and $p_c > 0$. Hence, we have the next result.

Proposition 3.2: *For $\varepsilon \to 0$, and for any x_0 with $-1 < x_0 < 1$, the hot-spot profile U_ε is stable on an $O(1)$ time-scale for any $\chi > 0$ and $p_c > 0$.*

3.2 The Eigenvalue Problem: An Exponentially Small Eigenvalue

In [4] and [6] it has been proved that (3.12) has an exponentially small eigenvalue λ_0 of the form $\lambda_0 = O(e^{-c/\varepsilon})$ as $\varepsilon \to 0$ for some $c > 0$. This must be the principal eigenvalue of the linearization.

We now use a similar method to that given in [14] to give a precise asymptotic estimate for λ_0. Using Proposition 3.1 for U_ε and I_0, we first write (3.12) more explicitly as

$$L_\varepsilon \phi \equiv \varepsilon^2 \phi_{xx} - 2\phi + 4w\phi - \frac{8w^2}{3\varepsilon\sqrt{2}} \int_{-1}^{1} w\phi \, dx = \lambda \phi \,, \quad |x| \le 1 \,, \tag{3.14a}$$

$$\phi_x(\pm 1) = 0 \,. \tag{3.14b}$$

Here $w = w(x)$ is defined by

$$w(x) \equiv \frac{3}{2} \mathrm{sech}^2 \left[\frac{\varepsilon^{-1}(x - x_0)}{\sqrt{2}} \right] . \tag{3.14c}$$

For $|x - x_0| \gg O(\varepsilon)$, $w(x)$ has the far field behavior

$$w(x) \sim 6 \, e^{-\sqrt{2}\varepsilon^{-1}|x - x_0|} \,, \qquad \text{for} \quad |x - x_0| \gg O(\varepsilon) \,. \tag{3.14d}$$

Let (λ_0, ϕ_0) be the principal eigenpair of (3.14). It is easy to see that $L_\varepsilon w_x$ is exponentially small, and that w_x fails to satisfy the boundary conditions in (3.14b) by only exponentially small terms as $\varepsilon \to 0$. This suggests that $\phi_0 \sim w_x$. We estimate λ_0 after constructing a boundary layer approximation to ϕ_0 in the form

$$\phi_0 \sim w_x + \phi_l \left[\varepsilon^{-1}(1 + x) \right] + \phi_r \left[\varepsilon^{-1}(1 - x) \right] \,. \tag{3.15}$$

Substituting (3.15) into (3.14a) and (3.14b), and using the far field behavior of $w(x)$ in (3.14d), we obtain that the boundary layer correction terms $\phi_l(\eta)$ and $\phi_r(\eta)$ satisfy

$$\phi_l'' - 2\phi_l = 0 \,, \qquad \eta \ge 0 \,; \qquad \phi_l'(0) \sim -12\varepsilon^{-1} e^{-\sqrt{2}(1 + x_0)/\varepsilon} \,, \tag{3.16a}$$

$$\phi_r'' - 2\phi_r = 0 \,, \qquad \eta \ge 0 \,; \qquad \phi_r'(0) \sim 12\varepsilon^{-1} e^{-\sqrt{2}(1 + x_0)/\varepsilon} \,. \tag{3.16b}$$

The solutions to (3.16) that are bounded as $\eta \to \infty$ are

$$\phi_l(\eta) = -\frac{\phi_l'(0)}{\sqrt{2}} e^{-\sqrt{2}\eta} \,, \qquad \phi_r(\eta) = -\frac{\phi_r'(0)}{\sqrt{2}} e^{-\sqrt{2}\eta} \,. \tag{3.17}$$

We now estimate the small eigenvalue λ_0. We define the inner product $(u, v) = \int_{-1}^{1} uv \, dx$. Multiplying both sides of the equation $L_\varepsilon \phi_0 = \lambda_0 \phi_0$ by w_x, we integrate by parts over the domain to get

$$\lambda_0 \, (w_x, \phi_0) = -\varepsilon^2 w_{xx} \phi_0 |_{-1}^{1} + (\phi_0, L_\varepsilon^* w_x) \,. \tag{3.18}$$

Here L_ε^* is the adjoint of the operator L_ε defined by

$$L_\varepsilon^*\phi \equiv \varepsilon^2\phi_{xx} - 2\phi + 4w\phi - \frac{8w}{3\varepsilon\sqrt{2}}\int_{-1}^{1} w^2\phi\,dx\,. \tag{3.19}$$

We now estimate each of the terms in (3.18). Using (3.14c) and (3.15), we calculate

$$(w_x, \phi_0) \sim \frac{9}{\varepsilon\sqrt{2}}\int_{-\infty}^{\infty} \mathrm{sech}^4 y\,\tanh^2 y\,dy = \frac{36}{15\varepsilon\sqrt{2}}\,. \tag{3.20}$$

Next, we use (3.14d), (3.15), and (3.17), to calculate the boundary term in (3.18) for $\varepsilon \ll 1$ as

$$-\varepsilon^2 w_{xx}\phi_0|_{-1}^{1} \sim \frac{144\sqrt{2}}{\varepsilon}\left[e^{-2\sqrt{2}(1+x_0)/\varepsilon} + e^{-2\sqrt{2}(1-x_0)/\varepsilon}\right]\,. \tag{3.21}$$

Finally, we calculate the last term on the right-hand side of (3.18). We obtain from (3.19) that

$$L_\varepsilon^* w_x = -\frac{8}{9\varepsilon\sqrt{2}}\left([w(1)]^3 - [w(-1)]^3\right) w(x)\,. \tag{3.22}$$

Therefore, using (3.15), we get

$$(\phi_0, L_\varepsilon^* w_x) \sim -\frac{4}{9\varepsilon\sqrt{2}}\left([w(1)]^3 - [w(-1)]^3\right)\left([w(1)]^2 - [w(-1)]^2\right)\,. \tag{3.23}$$

This term can be estimated using the far field form of w in (3.14d). For $\varepsilon \ll 1$, we get

$$(\phi_0, L_\varepsilon^* w_x) = O\left(\varepsilon^{-1}e^{-5\sqrt{2}b/\varepsilon}\right)\,, \qquad b = \mathrm{Min}(1+x_0, 1-x_0)\,. \tag{3.24}$$

Therefore, for $\varepsilon \ll 1$ this term is exponentially smaller than the boundary term (3.21). Hence, we can neglect this term in (3.18). Finally, the estimate for λ_0 is obtained by substituting (3.20) and (3.21) into (3.18). This leads to the next proposition.

Proposition 3.3: *For $\varepsilon \ll 1$, the exponentially small eigenvalue of (3.12) is given by*

$$\lambda_0 \sim 120\left(e^{-2\sqrt{2}(1-x_0)/\varepsilon} + e^{-2\sqrt{2}(1+x_0)/\varepsilon}\right)\,. \tag{3.25}$$

This estimate is independent of χ and p_c. A hot-spot equilibrium solution centered at the midpoint of the domain is unstable.

By symmetry, (3.3) has an equilibrium hot-spot solution centered at the origin $x_0 = 0$. However, since $\lambda_0 > 0$ in (3.25), this solution is unstable. As a partial verification of (3.25), we computed the exponentially small eigenvalue of (3.14) numerically for different values of ε when $x_0 = 0$ and compared the results with (3.25). The numerical computations were done using COLSYS [2]. In Fig. 11 we show this comparison graphically. In Table 3 we show a very favorable comparison between the asymptotic result (3.25) and the numerically computed values from (3.12).

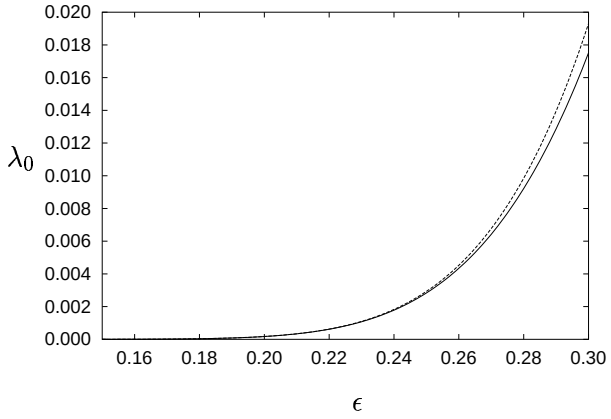

Figure 11: Comparison of numerical and asymptotic results for the calculation of the exponentially small eigenvalue of (3.14) when $x_0 = 0$. The full numerical results are given by the solid curve and the asymptotic results by the dotted curve.

3.3 The Metastable Dynamics

Since λ_0 is exponentially small in (3.25) when $\varepsilon \ll 1$, we expect that the location of the hot-spot moves exponentially slowly. We assume that at $t = 0$, a hot-spot is located at $x_0(0) = x_0^0$. The initial formation of this hot-spot, and its initial location, depends on the initial data for (3.3). This transient formation process was described qualitatively in [17]. Our goal is to derive a differential equation characterizing the subsequent evolution of the center of the hot-spot.

To derive a differential equation for the hot-spot location, we linearize (3.3) about the hot-spot profile U_ε, where the location of the hot-spot, $x_0 = x_0(t)$, is an unknown function of time. Since the linearization about the hot-spot profile has an exponentially small principal eigenvalue, we enforce the solvability condition that the full solution must be orthogonal to the projection on the eigenspace corresponding to the exponentially small eigenvalue. This leads to a differential equation for $x_0(t)$. A more detailed description of this projection method, and its application to other metastability problems, is given in [25].

We look for a solution to (3.3) near U_ε, where U_ε is defined in (3.9a) with $x_0 = x_0(t)$. We write

$$u(x,t) = U_\varepsilon[x; x_0(t)] + R(x,t)\,. \tag{3.26}$$

We assume that the residual R satisfies $R \ll U_\varepsilon$ and $R_t \ll \partial_t U_\varepsilon$. Substituting (3.26) into (3.3), we

ε	λ_0 (numerical)	λ_0 (asymptotic)
0.30	0.017515	0.0193038
0.28	0.0092211	0.00984407
0.26	0.0043407	0.00452595
0.23	0.0010745	0.00109514
0.20	0.00017189	0.000173125
0.18	0.35855×10^{-4}	0.359693×10^{-4}
0.16	0.50395×10^{-5}	0.504542×10^{-5}
0.14	0.40364×10^{-6}	0.403773×10^{-6}
0.10	0.12489×10^{-9}	0.124884×10^{-9}
0.08	0.10952×10^{-12}	0.106068×10^{-12}

Table 3: A comparison of the asymptotic and numerical values for λ_0 for different values of ε when $x_0 = 0$.

obtain that R satisfies the quasi steady-state problem

$$L_\varepsilon R = \partial_t U_\varepsilon \qquad |x| \le 1\,; \qquad R_x(\pm 1, t) = -\partial_x U_\varepsilon\left[\pm 1; x_0(t)\right]\,. \tag{3.27}$$

We multiply both sides of $L_\varepsilon R = \partial_t U_\varepsilon$ by ϕ_0, and integrate over the domain. Then, integrating the resulting expression by parts, we obtain

$$(\phi_0, \partial_t U_\varepsilon) = \varepsilon^2 \phi_0 R_x|_{-1}^{1} + (R, L_\varepsilon^* \phi_0)\,. \tag{3.28}$$

We now calculate each of the terms in (3.28). Since $\partial_t U_\varepsilon = -x_0' \gamma w_x$, we can use (3.15) and (3.20) to calculate

$$(\phi_0, \partial_t U_\varepsilon) \sim -\gamma x_0'\,(w_x, w_x) = -\frac{36 x_0' \gamma}{15\varepsilon\sqrt{2}}\,. \tag{3.29}$$

Here γ is defined in (3.9a). Next, we use (3.14d), (3.17), and (3.27), to obtain

$$\varepsilon^2 \phi_0 R_x|_{-1}^{1} \sim 144\gamma\left(e^{-2\sqrt{2}(1+x_0)/\varepsilon} - e^{-2\sqrt{2}(1-x_0)/\varepsilon}\right)\,. \tag{3.30}$$

In a similar way as shown in the estimation of λ_0 in (3.22)–(3.24), we can readily show that the last term on the right-hand side of (3.28) is exponentially smaller as $\varepsilon \to 0$ than the boundary term $\varepsilon^2 \phi_0 R_x|_{-1}^{1}$. Therefore, substituting (3.29) and (3.30) into (3.28), we obtain the following metastability result:

Proposition 3.4: *For $\varepsilon \ll 1$, a metastable hot-spot solution to (3.3) is given by*

$$u(x,t) \sim U_\varepsilon[x; x_0]\,, \qquad U_\varepsilon[x; x_0] \equiv \frac{3\gamma}{2}\mathrm{sech}^2\left(\frac{\varepsilon^{-1}[x - x_0(t)]}{\sqrt{2}}\right)\,, \tag{3.31a}$$

where the hot-spot location $x_0(t)$ satisfies the differential equation,

$$\frac{dx_0}{dt} \sim F(x_0) \equiv 60\varepsilon\sqrt{2}\left(e^{-2\sqrt{2}(1-x_0)/\varepsilon} - e^{-2\sqrt{2}(1+x_0)/\varepsilon}\right), \qquad x_0(0) = x_0^0 . \tag{3.31b}$$

Thus, the metastable behavior is, asymptotically, independent of χ and p_c.

This ODE shows that if $x_0^0 > 0$, then $x_0^{'} > 0$. Therefore, the hot-spot moves exponentially slowly towards the right boundary at $x = 1$. Alternatively, when $x_0^0 < 0$, the hot-spot moves exponentially slowly towards the left boundary at $x = -1$. Notice also, by comparing (3.25) and (3.31b), that $F^{'}(x_0) = 2\lambda_0$.

We now compare full numerical results for the evolution of a hot-spot, computed from (3.3), with the asymptotic dynamical behavior given in (3.31). The parameters are $p_c = \chi = 1$, and $\varepsilon = 0.1$, and the initial hot-spot location is $x_0(0) = -0.4$. The nonlocal problem (3.3) was solved numerically using a fourth order backward-differentiation scheme for the time-stepping, coupled with the solution to a boundary value problem at each time-step. COLSYS [2] was used to solve this boundary value problem. The numerical method is the same as was used in [14]. The results are shown in Fig. 12. From this figure we observe that the asymptotic result (3.31) closely approximates the hot-spot evolution from the full system (3.3).

Finally, we remark that the existence of metastable hot-spot behavior for (1.1) implies that the dynamical behavior for (1.1) will be sensitive to very small perturbations in the differential operator. Hence, in a physical experiment one may observe somewhat different hot-spot dynamics. In particular, for a slightly nonuniform sample where the diffusivity is a very slowly varying function of x, there will be a competition between the dynamical law (3.31) and another term that is proportional to the spatial derivative of the diffusivity. The overall effect can lead to new equilibrium hot-spot locations. This type of very weak pinning effect has been analyzed in detail in [16] for a spike solution to the Gierer-Meinhardt model.

3.4 A Generalized Polynomial Conductivity Model

Next, we briefly determine the effect on the hot-spot profile and the stability of this profile for a generalized polynomial conductivity model of the form

$$f(u) = 1 + c_1 u^p . \tag{3.32}$$

Here $c_1 > 0$ and $p > 1$.

Repeating the calculations from (3.1)–(3.8) for this conductivity model, we obtain the following result, analogous to Proposition 3.1, for the hot-spot profile:

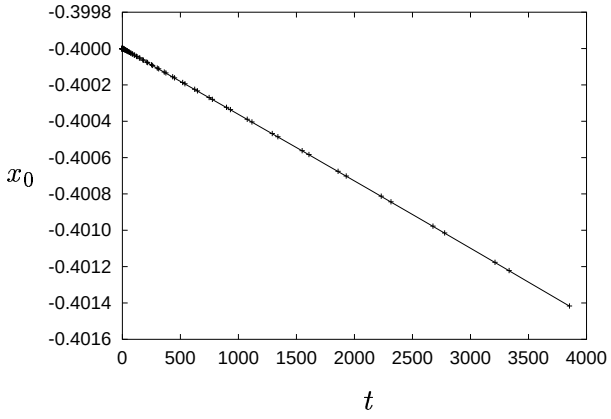

Figure 12: Comparison of numerical and asymptotic results for the hot-spot location $x_0(t)$ when $p_c = \chi = 1$ and $\varepsilon = 0.1$. The full numerical result is the dotted curve and the asymptotic results from (3.31) are the cross points.

Proposition 3.5: *Let $\varepsilon \to 0$ and suppose that the Biot number b satisfies $b \ll \varepsilon^{6/(p+1)}$ in (3.1). Then, the hot-spot profile for (3.1) has the form $u \sim \varepsilon^{-2/(p+1)} U_\varepsilon$, where $= U_\varepsilon[x; x_0]$ is given by*

$$U_\varepsilon[x; x_0] \equiv \gamma w\left[\sqrt{2}\varepsilon^{-1}(x - x_0)\right] , \tag{3.33a}$$

$$\gamma \equiv \left(\frac{p_c}{\beta_p^2 c_1 \chi^2}\right)^{1/(p+1)} , \qquad \beta_p \equiv \int_{-\infty}^{\infty} [w(\xi)]^p \, d\xi \, . \tag{3.33b}$$

Here $w(\xi)$ is the solution to (2.12) on the infinite line, which was given explicitly in (2.14).

To derive the eigenvalue problem that determines the stability of the hot-spot profile, we proceed as in (3.11)-(3.12). In place of (3.13), we now obtain that

$$\Phi_{\xi\xi} - \Phi + p w^{p-1}\Phi - \alpha w^p \left(\frac{\int_{-\infty}^{\infty} w^{p-1}\Phi \, d\xi}{\int_{-\infty}^{\infty} w^p \, d\xi}\right) = \frac{\lambda}{2}\Phi \, , \qquad -\infty < \xi < \infty \, , \tag{3.34a}$$

where $\Phi \to 0$ as $|\xi| \to \infty$, and α is given by

$$\alpha = 2p \, . \tag{3.34b}$$

Notice that the hot-spot profile depends on the parameter c_1 in the conductivity model, but that the stability property of this profile is independent of c_1 when $\varepsilon \ll 1$. Notice also that for

the case studied in §3.1–3.3 where $p = 2$, the multiplier α of the nonlocal term is $\alpha = 4$, and Proposition 3.2 follows. The case $p = 3$ was Example 3 in §2.2.

To show that the hot-spot profile is stable, one must show that there is no eigenvalue of (3.34) in the right half-plane. We have used the finite difference method of §2.2 to show numerically that stability holds for the integer values $p = 3, 4, 5, 6, 7$. A rigorous proof of stability for (3.34) appears in [28] as a consequence of a stability analysis for a fractional power reaction-diffusion system. Therefore, hot-spot profiles are stable for any conductivity model of the form $f(u) = 1 + c_1 u^p$.

4 Pinning for the Model Problem

In this section we construct a hot-spot solution for (1.2) for in the limit $\varepsilon \to 0$ for the conductivity profile $f(u) = 1 + u^2$. For this model, metastable hot-spot behavior does not occur. Instead, we will show that the dynamics of a hot-spot will get pinned on a long $O(\varepsilon^{-2})$ time-scale to a local maximum of the function $g(x)$ in (1.2).

As in the study of (1.1) in §3, a hot-spot solution u for (1.2) will will tend to ∞ as $\varepsilon \to 0$ in an $O(\varepsilon)$ region of the hot-spot location x_0 (cf. [5]). We thus re-scale u so that the maximum of the temperature is bounded as $\varepsilon \to 0$. The appropriate scaling in (1.2) is again $u = \varepsilon^{-2/3} U$. With this scaling, and assuming as before that $b \ll \varepsilon^2$, we obtain from (1.2) that U satisfies

$$U_t = \varepsilon^2 U_{xx} - 2U + \frac{p_c g(x) U^2}{\chi^2 I_\varepsilon^2}\,, \quad |x| \le 1\,; \qquad U_x(\pm 1, t) = 0\,, \tag{4.1a}$$

where

$$I_\varepsilon = \varepsilon^{-1} \int_{-1}^{1} g(x) U^2 \, dx\,. \tag{4.1b}$$

We first construct the hot-spot profile. Since the asymptotic construction of this profile is very similar to that given in §3, we omit the details of this analysis. The following asymptotic result is obtained:

Proposition 4.1: *Let $\varepsilon \to 0$ and assume that $g(x_0) > 0$. Then, the hot-spot profile U_ε is given by*

$$U \sim U_\varepsilon[x; x_0] \equiv \gamma w\left[\sqrt{2}\varepsilon^{-1}(x - x_0)\right]\,, \qquad \gamma \equiv \left(\frac{p_c}{36\, g(x_0)\chi^2}\right)^{1/3}\,. \tag{4.2a}$$

Here $w(\xi)$ is the solution to (3.7) given in (3.9b). For $\varepsilon \to 0$, the nonlocal term I_ε in (4.1b) is

$$I_\varepsilon \sim 3\sqrt{2} g(x_0) \left(\frac{p_c}{36\, g(x_0)\chi^2}\right)^{2/3} + O(\varepsilon)\,. \tag{4.2b}$$

The stability of the hot-spot profile for a fixed value $x_0 \in (-1,1)$ can be analyzed in exactly the same way as in §3.1. Substituting

$$U = \gamma w(\xi) + \Phi(\xi) e^{\lambda t}\,, \qquad \xi \equiv \sqrt{2}\varepsilon^{-1}(x - x_0)\,, \tag{4.3}$$

into (4.1), we readily obtain the nonlocal eigenvalue problem (3.13a). The constant α in (3.13a) is

$$\alpha = \frac{6\sqrt{2}\, p_c\, [g(x_0)]^2 \gamma^3}{\chi^2 I_\varepsilon^3}\,. \tag{4.4}$$

From Proposition 2.3, we conclude that the profile is stable on an $O(1)$ time-scale if and only if $\alpha > 1$. Using (4.2) for γ and I_ε, we calculate $\alpha = 4$. This proves the stability of the hot-spot profile for any $x_0 \in (-1,1)$. It is important to note that Proposition 2.3 pertains only to eigenvalues of the linearization that are $O(1)$ as $\varepsilon \to 0$. For (1.1) we had to determine by a different analysis the sign of any eigenvalues that tend to zero as $\varepsilon \to 0$. These eigenvalues are usually called the critical eigenvalues. For (1.1) there is such an eigenvalue that is exponentially small as $\varepsilon \to 0$. For (1.2) we show below that a critical eigenvalue is $O(\varepsilon^2)$ as $\varepsilon \to 0$.

Next, we derive a differential equation for the location of a hot-spot for (1.2). We assume that at $t = 0$, the hot-spot is located at $x_0(0) = x_0^0 \in (-1,1)$ and that the initial condition for U has the form of a hot-spot profile. The transient process of hot-spot formation is discussed qualitatively, and computed numerically, in [18]. The equilibria of the resulting differential equation for x_0 determine the equilibrium locations for hot-spot solutions of (1.2). The critical eigenvalues for the linearization of (4.1) around an equilibrium hot-spot solution are obtained directly from this differential equation. In the analysis below, we allow $g(x)$ to be an arbitrary positive function.

To determine the dynamical behavior of x_0 we expand the solution to (4.1) as

$$U = \gamma w(\xi) + \varepsilon w_1(\xi) + \cdots\,, \tag{4.5a}$$

where

$$\xi = \sqrt{2}\varepsilon^{-1}\left[x - x_0(\tau)\right]\,, \qquad \tau \equiv \varepsilon^2 t\,. \tag{4.5b}$$

Substituting (4.5) into the nonlocal term I_ε given in (4.1b), and using $\int_{-\infty}^{\infty} \xi w^2\, d\xi = 0$, we obtain

$$I_\varepsilon = 3\sqrt{2}\, g(x_0)\, \gamma^2 \left[1 + \frac{\varepsilon}{3\gamma}\int_{-\infty}^{\infty} w w_1\, d\xi + O(\varepsilon^2)\right]\,. \tag{4.6}$$

We substitute (4.5) and (4.6) into (4.1) and collect powers of ε. From the $O(1)$ terms we obtain that $w(\xi)$ satisfies (3.7). From the $O(\varepsilon)$ terms, and after using the formula for γ in (4.2a), we

obtain that w_1 satisfies

$$\mathcal{A}w_1 \equiv w_{1\xi\xi} - w_1 + 2ww_1 - \frac{2w^2}{3}\int_{-\infty}^{\infty} ww_1\,d\xi = -\frac{\gamma}{\sqrt{2}}\left[x_0' w_\xi + \xi w^2\left(\frac{g'(x_0)}{g(x_0)}\right)\right], \qquad -\infty < \xi < \infty, \tag{4.7}$$

with $w_1 \to 0$ as $\xi \to \pm\infty$. Here $x_0' \equiv dx_0/d\tau$.

In order to determine w_1 we must impose a solvability condition on the right-hand side of (4.7). Since w_ξ is in the null-space of the adjoint operator $\mathcal{A}^*$, the solvability condition for (4.7) is that the right-hand side of (4.7) is orthogonal to w_ξ. This yields that x_0 satisfies

$$x_0'\int_{-\infty}^{\infty} w_\xi^2\,d\xi = -\left(\frac{g'(x_0)}{g(x_0)}\right)\int_{-\infty}^{\infty}\xi w^2 w_\xi\,d\xi\,. \tag{4.8}$$

Upon integrating the right-hand side of (4.8) by parts, and using $w = \frac{3}{2}\mathrm{sech}^2(\xi/2)$ to evaluate the resulting integrals, we obtain the following main result:

Proposition 4.2: *Let $\varepsilon \to 0$ and assume that $g(x_0) > 0$. Then, the dynamical behavior of a hot-spot solution for (1.2) is given by*

$$U \sim \frac{3\gamma}{2}\mathrm{sech}^2\left(\frac{\varepsilon^{-1}[x - x_0(t)]}{\sqrt{2}}\right), \qquad \gamma \equiv \left(\frac{p_c}{36g\,[x_0(t)]\,\chi^2}\right)^{1/3}, \tag{4.9a}$$

where the hot-spot location $x_0(t)$ satisfies the differential equation,

$$\frac{dx_0}{dt} \sim 2\varepsilon^2\left(\frac{g'(x_0)}{g(x_0)}\right). \tag{4.9b}$$

From (4.9b) we conclude that equilibrium hot-spot locations are at critical points of $g(x_0)$. Let $g'(x_e) = 0$. Then, from (4.9b), the local growth rate near the equilibrium point x_e is

$$\lambda_0 = 2\varepsilon^2\left(\frac{g''(x_e)}{g(x_e)}\right). \tag{4.10}$$

This determines the critical eigenvalue. Hence, stable equilibrium hot-spot locations are at non-degenerate local maxima of $g(x)$. Physically this implies that there will be a stable hot-spot equilibrium solution centered at any local maximum of the electric field. For the $g(x)$ as given in (1.2b), we obtain that the hot-spot location satisfies

$$\frac{dx_0}{dt} \sim -\pi\varepsilon^2\frac{\sin(\pi x_0)}{\cos^2(\frac{\pi}{2}x_0)}. \tag{4.11}$$

Hence, $x_0 \to 0$ as $t \to \infty$ for any $x_0(0) \in (-1, 1)$.

From (4.11) we observe that the dynamics of a hot-spot solution for (4.1) is, asymptotically, independent of p_c and χ when $\varepsilon \ll 1$. For the $g(x)$ of (1.2b), in Fig. 13(a) we compare full numerical results for the evolution of a hot-spot, computed from (4.1), with the asymptotic dynamical behavior given in (4.11). In (4.1) and (4.11) we took $p_c = 1$, $\chi = 1$, and $\varepsilon = 0.1$. The initial condition for (4.1) was the hot-spot profile (4.9a) with $x_0(0) = -0.4$. The nonlocal problem (4.1) was solved numerically using the approach outlined in §3.3. The solution U is plotted at three different times in Fig. 13(b). The comparison shown in Fig. 13(a) illustrates that the asymptotic result (4.11) closely approximates the hot-spot evolution from the full system (4.1) even when ε is not too small.

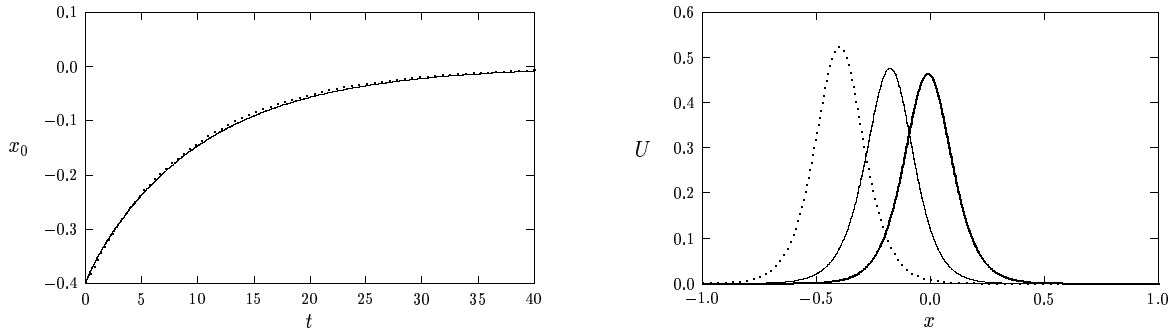

(a) x_0 versus t

(b) U versus x

Figure 13: Left figure: The hot-spot location $x_0(t)$ for $p_c = \chi = 1$, and $\varepsilon = 0.1$. The full numerical result is the solid curve, and the asymptotic result (4.11) is the dashed curve. Right figure: The solution U to (4.1) at $t = 0$ (dashed curve), $t = 8.1$ (solid curve), and $t = 40.0$ (heavy solid curve).

5 Metastability and Pinning for the Microwave Heating Problem

In this section we analyze the dynamics of hot-spot solutions for the conductivity model $f(u) = e^{c_1 u}$ of (1.3). Although the analysis is similar to that in §3 and §4 for the case $f(u) = (1 + u^2)$, the asymptotic construction of the homoclinic orbit is significantly more intricate here owing to the interplay between algebraic and logarithmic terms in ε. In §5.1 we analyze metastable behavior for (1.1), while in §5.2 we study the pinning phenomena associated with (1.2).

5.1 Metastability: The Exponential Conductivity Model

In the analysis below we assume that $b \ll 1$ in (1.1). Our asymptotic analysis used to construct the homoclinic orbit follows closely the approach used in [17]. In terms of $y = \varepsilon^{-1}(x - x_0)$, the homoclinic solution for (1.1) satisfies

$$v_{yy} - 2v + \Gamma_0 f(v) = 0\,, \qquad -\infty < y < \infty\,, \tag{5.1a}$$

$$v_y(0) = 0\,; \qquad v \to \sigma \quad \text{as} \quad |y| \to \infty\,, \tag{5.1b}$$

where $f(v) = e^{c_1 v}$, and

$$\Gamma_0 \equiv \frac{p_c}{1 + \chi^2 I_0^2}\,, \qquad I_0 \equiv \int_{-1}^{1} f\left(v\left[\varepsilon^{-1}(x - x_0)\right]\right)\, dx\,. \tag{5.1c}$$

In (5.1b), σ is the root of

$$2\sigma = \Gamma_0 f(\sigma)\,, \tag{5.1d}$$

for which $2 > \Gamma_0 f'(\sigma)$. Let $v(0) = v_m$ denote the maximum of v. In [17] it was shown that (5.1) has a solution with $v_m \to \infty$ as $\varepsilon \to 0$. Consequently, from (5.1c), we have $I_0 \to \infty$, and $\Gamma_0 \to 0$ as $\varepsilon \to 0$. From (5.1d), this implies that $\sigma \to 0$ as $\varepsilon \to 0$. We now estimate these terms precisely.

Since $v_m \to \infty$ as $\varepsilon \to 0$, we follow [17] and use Laplace's method to estimate I_0. In the resulting formula, we use (5.1a) to calculate $v_{yy}(0)$. This yields,

$$I_0 \sim \varepsilon e^{c_1 v_m} \sqrt{\frac{2\pi}{c_1 |v_{yy}(0)|}} = e^{c_1 v_m} \sqrt{\frac{2\pi}{c_1\left(\Gamma_0 e^{c_1 v_m} - 2v_m\right)}}\,. \tag{5.2}$$

Substituting (5.2) into (5.1c), we obtain an equation for Γ_0. This equation can be solved to get

$$\Gamma_0 \sim 2\beta v_m e^{-c_1 v_m}\left[\beta - e^{c_1 v_m + 2\log\varepsilon}\right]^{-1}\,, \qquad \beta \equiv \frac{p_c c_1}{2\pi\chi^2}\,. \tag{5.3}$$

To obtain an additional equation for Γ_0, we determine the first integral of (5.1a) as

$$\frac{1}{2}v_y^2 - v^2 + \frac{\Gamma_0}{c_1} e^{c_1 v} = -\sigma^2 + \frac{\Gamma_0}{c_1} e^{c_1 \sigma}\,. \tag{5.4}$$

Next, we evaluate (5.4) at $y = 0$, and use $v(0) = v_m$ and $\sigma \ll 1$, to get

$$\Gamma_0 \sim c_1 v_m^2 e^{-c_1 v_m}\,. \tag{5.5}$$

Eliminating Γ_0 between (5.3) and (5.5) we get a transcendental equation for v_m in the form

$$e^{c_1 v_m + 2\log\varepsilon} \sim \beta\left(1 - \frac{2}{c_1 v_m}\right)\,. \tag{5.6}$$

For $\varepsilon \ll 1$, it follows readily that (5.6) has a unique root given asymptotically by

$$v_m \sim \frac{1}{c_1}\log\left(\frac{\beta}{\varepsilon^2}\right) + \frac{1}{c_1}\log\left[1 - \frac{2}{\log\left(\beta/\varepsilon^2\right)}\right] + \dots \,. \tag{5.7}$$

Finally, we use (5.7) to calculate I_0 and Γ_0 asymptotically from (5.2) and (5.3), respectively. We get

$$\Gamma_0 \sim \frac{c_1 v_m^2 \varepsilon^2}{\beta}\left[1 - \frac{2}{\log\left(\beta/\varepsilon^2\right)}\right]^{-1}, \qquad I_0 \sim \frac{\beta}{\varepsilon}\left[1 - \frac{2}{\log\left(\beta/\varepsilon^2\right)}\right]\sqrt{\frac{2\pi}{c_1 v_m\left(c_1 v_m - 2\right)}}\,. \tag{5.8}$$

Hence $\Gamma_0 = O\left(\varepsilon^2\left[\log\varepsilon\right]^2\right)$, and $I_0 = O\left(\varepsilon^{-1}\left[\log\varepsilon\right]^{-1}\right)$. From (5.1d), we then calculate σ as

$$\sigma \sim \frac{\Gamma_0}{2}\exp\left(\frac{c_1\Gamma_0}{2}\right) = O\left(\varepsilon^2\left[\log\varepsilon\right]^2\right)\,. \tag{5.9}$$

The hot-spot profile $U_\varepsilon[x;x_0]$ is then defined by

$$U_\varepsilon[x;x_0] \equiv v\left[\varepsilon^{-1}(x - x_0)\right]\,. \tag{5.10}$$

The far-field behavior of $v(y)$ as $|y| \to \infty$ is central to the metastability analysis. We write (5.1a) as $v_{yy} + q(v) = 0$, where $q(v) \equiv -2v + \Gamma_0 f(v)$, where $f(v) = e^{c_1 v}$. The far field behavior for $v(y)$ has the form

$$v(y) \sim \sigma + a e^{-\nu|y|}\,, \quad \text{as} \quad |y| \to \infty\,, \tag{5.11a}$$

where $\nu > 0$ and $a > 0$ are to be found, and σ satisfies (5.1d). In the analysis below, we must also calculate $\int_{-\infty}^{\infty} v_y^2\, dy$. These constants were determined for a general $q(v)$ in [24]. Applying the result of [24] to this problem, we obtain the explicit formulae

$$\nu \equiv \left[-q'(\sigma)\right]^{1/2} = \left[2(1 - c_1\sigma)\right]^{1/2} = \sqrt{2} + O\left(\varepsilon^2\left[\log\varepsilon\right]^2\right)\,, \tag{5.11b}$$

$$\log a \equiv \log(v_m - \sigma) + \int_\sigma^{v_m}\left(\frac{\nu}{\left[-2Q(\eta)\right]^{1/2}} - \frac{1}{\eta - \sigma}\right)d\eta\,, \tag{5.11c}$$

$$\int_{-\infty}^{\infty}\left[v_y(y)\right]^2\, dy = 2\int_\sigma^{v_m}\left[-2Q(v)\right]^{1/2}\, dv\,. \tag{5.11d}$$

Here $Q(v) \equiv \int_\sigma^v q(\eta)\, d\eta$, and $v_m = v(0)$ is the maximum of $v(y)$. An important feature of these formulae are that they can be calculated without having an explicit pointwise expression for the homoclinic orbit $v(y)$.

ε	v_m	Γ_0	a	ν	$\int_{-\infty}^{\infty} v_y^2\,dy$
0.40	5.97	0.698×10^{-2}	1.76	1.4105	42.2
0.35	6.15	0.563×10^{-2}	1.82	1.4112	45.2
0.30	6.36	0.439×10^{-2}	1.85	1.4119	48.6
0.25	6.66	0.326×10^{-2}	1.88	1.4125	53.0
0.20	6.91	0.226×10^{-2}	1.93	1.4130	58.5
0.15	7.31	0.140×10^{-2}	1.99	1.4135	65.9
0.10	7.86	0.708×10^{-3}	2.06	1.4138	77.1

Table 4: Numerical values for the homoclinic orbit constants at different values of ε for the exponential conductivity model $f(u) = e^{c_1 u}$, with $p_c = 0.66$, $\chi = 0.01$, and $c_1 = 1.5$.

In summary, the homoclinic orbit satisfies (5.1), where $v(0) = v_m$, Γ_0, and σ, are given asymptotically in (5.7), (5.8), and (5.9), respectively. In terms of these values, we can then compute a, ν, and $\int_{-\infty}^{\infty} v_y^2\,dy$ from (5.11). In Table 4 we give numerical values for these quantities at different values of ε for the realistic parameter values $p_c = 0.66$, $\chi = 0.01$, and $c_1 = 1.5$, that were used in [17] and [18].

We now study the metastable behavior. Assuming that the initial data for (1.1) has the form of a hot-spot profile, we write $u(x,t)$ as in (3.26). Substituting this form into (1.1), we obtain the quasi-steady state problem (3.27), where the operator L_ε in (3.27) is now defined by

$$L_\varepsilon \phi \equiv \varepsilon^2 \phi_{xx} - \left[2 - c_1 \Gamma_0 f(v)\right] \phi - \alpha f(v) \int_{-1}^{1} f(v)\phi\,dx\,. \tag{5.12}$$

Here $v = v\left[\varepsilon^{-1}(x - x_0)\right]$ satisfies (5.1), and α is given by

$$\alpha \equiv \left(\frac{2\chi^2 c_1}{p_c}\right) \Gamma_0^2\, I_0\,. \tag{5.13}$$

In [4] it was proved that the eigenvalue problem $L_\varepsilon \phi = \lambda\phi$, with $\phi_x(\pm 1) = 0$, has an exponentially small principal eigenvalue λ_0 as $\varepsilon \to 0$. However, no precise estimate for λ_0 was given.

We now estimate λ_0. The corresponding eigenfunction ϕ_0 is given asymptotically by

$$\phi_0 \sim v_x + \phi_l\left[\varepsilon^{-1}(1 + x)\right] + \phi_r\left[\varepsilon^{-1}(1 - x)\right]\,. \tag{5.14}$$

To determine the boundary layer functions ϕ_l and ϕ_r, we use the far-field behavior (5.11a) for v in satisfying the boundary conditions $\phi_{0x}(\pm 1) = 0$. We then proceed as in (3.16)–(3.17) to get

$$\phi_0(-1) \sim 2\varepsilon^{-1} a\nu e^{-\nu(1+x_0)/\varepsilon}\,, \qquad \phi_0(+1) \sim -2\varepsilon^{-1} a\nu e^{-\nu(1-x_0)/\varepsilon}\,. \tag{5.15}$$

Then, since L_ε is self-adjoint, we obtain in in place of (3.18) that

$$\lambda_0 \, (v_x, \phi_0) = -\varepsilon^2 v_{xx} \phi_0|_{-1}^1 + (\phi_0, L_\varepsilon v_x) \; . \tag{5.16}$$

As in §3 we can show that the second term on the right-hand side of (5.16) is asymptotically negligible in comparison with the boundary term in (5.16). Finally, substituting (5.11a), (5.14), and (5.15), into (5.16) we obtain the following result:

Proposition 5.1: *For $\varepsilon \to 0$, and for the conductivity model $f(u) = e^{c_1 u}$, the exponentially small eigenvalue λ_0 of the operator L_ε in (5.12) is given by*

$$\lambda_0 \sim \frac{2a^2\nu^3}{\left(\int_{-\infty}^{\infty} [v_y(y)]^2 \; dy \right)} \left(e^{-2\nu(1-x_0)/\varepsilon} + e^{-2\nu(1+x_0)/\varepsilon} \right) \; . \tag{5.17}$$

Here v satisfies (5.1), with ν and a defined in (5.11b) and (5.11c), respectively.

To derive a differential equation for the hot-spot location $x_0(t)$, we multiply (3.27) by ϕ_0 to obtain (3.28) where L_ε^* in (3.28) is replaced by L_ε. We use $\partial_t U_\varepsilon = -\varepsilon^{-1} x_0' v_y$ to calculate the inner product term on the left-hand side of (3.28), and (5.11a) and (5.15) to calculate the boundary term in (3.28). In this way, we obtain

$$\varepsilon^2 \phi_0 R_x|_{-1}^1 \sim 2a^2\nu^2 \left(e^{-2\nu(1+x_0)/\varepsilon} - e^{-2\nu(1-x_0)/\varepsilon} \right) \; , \qquad (\phi_0, \partial_t U_\varepsilon) \sim -\varepsilon^{-1} x_0' \int_{-\infty}^{\infty} [v_y(y)]^2 \; dy \, . \tag{5.18}$$

Substituting (5.18) into (3.28), we obtain the following metastability result:

Proposition 5.2: *For $\varepsilon \ll 1$, and for the conductivity model $f(u) = e^{c_1 u}$, the hot-spot solution to (1.1) is given by (5.10), where the hot-spot location $x_0(t)$ satisfies the differential equation*

$$\frac{dx_0}{dt} \sim \varepsilon \zeta \left(e^{-2\nu(1-x_0)/\varepsilon} - e^{-2\nu(1+x_0)/\varepsilon} \right) \; , \qquad \zeta \equiv \frac{2a^2\nu^2}{\left(\int_{-\infty}^{\infty} [v_y(y)]^2 \; dy \right)} \, , \tag{5.19}$$

with initial condition $x_0(0) = x_0^0$.

Since $\nu \sim \sqrt{2}$ as $\varepsilon \to 0$, we observe from Propositions 3.3, 3.4, 5.1, and 5.2, that apart from a difference in the pre-exponential multiplicative factors, the asymptotic estimates for λ_0 and dx_0/dt are very similar for both the polynomial and the exponential conductivity models. The term ζ in (5.19) can be evaluated numerically from (5.11) or Table 4. As an example, we take the realistic parameter set $p_c = 0.66$, $\chi = 0.01$, and $c_1 = 1.5$, of [17] and [18]. For a hot-spot located initially at $x_0(0) = -0.4$, and for three values of ε, we compute the hot-spot trajectory from (5.19). The results are shown in Fig. 14 in the form $\log_{10}(t+1)$ versus x_0.

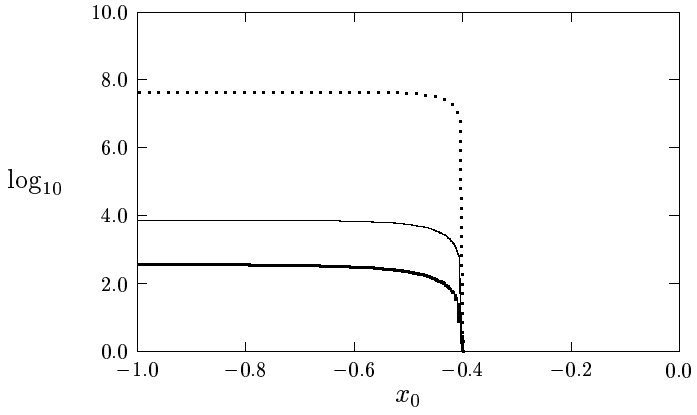

Figure 14: Plots of $\log_{10}(t+1)$ versus x_0 computed from (5.19) when $p_c = 0.66$, $\chi = 0.01$, and $c_1 = 1.5$. The values of ε are $\varepsilon = 0.3$ (heavy solid curve), $\varepsilon = 0.2$ (solid curve), and $\varepsilon = 0.1$ (dashed curve).

5.2 Pinning: The Exponential Conductivity Model

We now analyze (1.2) for the conductivity model $f(u) = e^{c_1 u}$. As in §5.1, we assume that $b \ll 1$ in (1.2). In (1.2), we allow $g(x)$ to be any smooth function with $g(x) > 0$ on $-1 < x < 1$. We first construct the homoclinic orbit when the hot-spot is at $x = x_0$. In terms of $y = \varepsilon^{-1}(x - x_0)$, the leading order homoclinic solution for (1.2) satisfies

$$v_{yy} - 2v + \Gamma_0 g(x_0) f(v) = 0\,, \qquad -\infty < y < \infty\,, \tag{5.20a}$$

$$v_y(0) = 0\,; \qquad v \to \sigma \quad \text{as} \quad |y| \to \infty\,, \tag{5.20b}$$

where $f(v) = e^{c_1 v}$, and

$$\Gamma_0 = \frac{p_c}{(1+\chi I_0)^2}\,, \qquad I_0 = \int_{-1}^{1} g(x) f\left(v\left[\varepsilon^{-1}(x-x_0)\right]\right)\,dx\,. \tag{5.20c}$$

In (5.20b), σ is the root of

$$2\sigma = \Gamma_0 g(x_0) f(\sigma)\,, \tag{5.20d}$$

which tends to zero as $\Gamma_0 \to 0$. The outer steady-state solution $u_0(x)$ for (1.2), away from the hot-spot region, satisfies $2u_0 = \Gamma_0 g(x) f(u_0)$. The matching condition is that $\sigma = u_0(x_0)$. Let

$v(0) = v_m$ denote the maximum of v. As in §5.1, the hot-spot profile has the limiting behavior $v_m \to \infty$, $I_0 \to \infty$, $\Gamma_0 \to 0$, and $\sigma \to 0$, as $\varepsilon \to 0$.

Since the analysis to construct the hot-spot profile parallels that given in §5.1, we only give the asymptotic estimates for v_m, I_0, Γ_0, and σ_0. In place of (5.6) we obtain that v_m satisfies the transcendental equation

$$e^{c_1 v_m + 2\log\varepsilon} \sim \frac{\beta}{g(x_0)}\left(1 - \frac{2}{c_1 v_m}\right), \tag{5.21}$$

where β is defined in (5.3). Consequently, for $\varepsilon \ll 1$ we get

$$v_m \sim \frac{1}{c_1}\log\left(\frac{\beta}{g(x_0)\varepsilon^2}\right) + \frac{1}{c_1}\log\left(1 - \frac{2}{\log\left[\beta/(g(x_0)\varepsilon^2)\right]}\right) + \dots . \tag{5.22}$$

In place of (5.8) we now obtain

$$\Gamma_0 \sim \frac{c_1 v_m^2 \varepsilon^2}{\beta}\left(1 - \frac{2}{\log\left[\beta/(g(x_0)\varepsilon^2)\right]}\right)^{-1}, \quad I_0 \sim \frac{\beta}{\varepsilon}\left(1 - \frac{2}{\log\left[\beta/(g(x_0)\varepsilon^2)\right]}\right)\sqrt{\frac{2\pi}{c_1 v_m\left(c_1 v_m - 2\right)}}. \tag{5.23}$$

Finally, we estimate

$$\sigma \sim \frac{\Gamma_0\, g(x_0)}{2}\exp\left(\frac{c_1\Gamma_0 g(x_0)}{2}\right). \tag{5.24}$$

Next, we determine the dynamics of a hot-spot solution. We write (1.2), with $b = 0$, as

$$u_t = \varepsilon^2 u_{xx} - 2u + \Gamma g(x) f(u), \quad |x| \le 1; \qquad u_x(\pm 1, t) = 0, \tag{5.25a}$$

where $f(u) = e^{c_1 u}$. Here Γ is defined by

$$\Gamma \equiv \frac{p_c}{(1+\chi I)^2}, \qquad I \equiv \int_{-1}^{1} g(x) f(u)\, dx. \tag{5.25b}$$

We look for a solution to (5.25) in the form

$$u = v(y) + \varepsilon w_1(y) + \dots, \qquad y = \varepsilon^{-1}\left[x - x_0(\tau)\right], \quad \tau = \varepsilon^2 t, \tag{5.26}$$

with $w_1 \to 0$ as $|y| \to \infty$. Expanding Γ in powers of ε we obtain

$$\Gamma = \Gamma_0 + \varepsilon\Gamma_1 + \dots, \qquad \Gamma_1 \equiv -\frac{2\chi\Gamma_0}{1+\chi I_0}\int_{-1}^{1} g(x) f'(v) w_1\, dx. \tag{5.27}$$

Here Γ_0 and I_0 are defined in (5.20c). Substituting (5.26) and (5.27) into (5.25a), and using $g(x) = g(x_0) + \varepsilon y g'(x_0) + \dots$, we collect the $O(\varepsilon)$ terms to obtain

$$\mathcal{A}w_1 \equiv w_{1yy} - 2w_1 + \Gamma_0 g(x_0) f'(v) w_1 - \kappa g(x_0) f(v)\int_{-1}^{1} g(x) f(v) w_1\, dx = -x_0' v_y - g'(x_0) y \Gamma_0 f(v), \tag{5.28a}$$

where κ is defined by

$$\kappa \equiv \frac{2\chi\Gamma_0 c_1}{1+\chi I_0}\,. \tag{5.28b}$$

The operator $\mathcal{A}$ is self-adjoint. To determine a differential equation for x_0 we require that the right-hand side of (5.28a) is orthogonal to the null-space of $\mathcal{A}$. Let $\mathcal{A}_l$ be the local part of the operator in (5.28a). Then, by translation invariance, $\mathcal{A}_l v_y = 0$, where v satisfies (5.20). We now estimate that $\mathcal{A}v_y = O\left[\varepsilon^2(\log\varepsilon)^2\right]$. To show this, we first use Laplace's method and the fact that v_y is odd to get

$$\int_{-1}^{1} g(x)f(v)v_y\,dx \sim \varepsilon\int_{-\infty}^{\infty}\left[g(x_0)+\varepsilon g'(x_0)y\right]f(v)v_y\,dy \sim \varepsilon^2 g'(x_0)\int_{-\infty}^{\infty} y e^{c_1 v}v_y\,dy = O\left(\frac{1}{\log\varepsilon}\right). \tag{5.29}$$

Now let C be a generic $O(1)$ constant. From (5.22) and (5.23) we estimate $|f(v)| \le C\varepsilon^{-2}$ for $-\infty < y < \infty$, and $\kappa = O\left(\Gamma_0/I_0\right) = O\left[\varepsilon^4(\log\varepsilon)^3\right]$. Combining these estimates we obtain the desired result $\mathcal{A}v_y = O\left[\varepsilon^2(\log\varepsilon)^2\right]$. This implies that v_y is, asymptotically, an element in the null-space of $\mathcal{A}$. Although, in principle, we can improve our approximation to the null-space of $\mathcal{A}$ by calculating correction terms to v_y, this is not necessary for our leading order calculation of the speed x_0'.

Asymptotically, the right-hand side of (5.28a) must be orthogonal to v_y. This determines $dx_0/d\tau$ with $\tau = \varepsilon^2 t$, and yields the following result:

Proposition 5.3: *Let $g(x_0) > 0$. Then for $\varepsilon \ll 1$, and for the conductivity model $f(u) = e^{c_1 u}$, the hot-spot location $x_0(t)$ satisfies*

$$\frac{dx_0}{dt} \sim \frac{\varepsilon^2 g'(x_0)\Gamma_0 J}{\left(\int_{-\infty}^{\infty}\left[v_y(y)\right]^2\,dy\right)}\,, \qquad J \equiv -\int_{-\infty}^{\infty} y e^{c_1 v}v_y\,dy\,. \tag{5.30}$$

Since $J > 0$, we observe that stable equilibrium hot-spot locations are at local maxima of $g(x_0)$. We can cast our result in a more explicit form by using Laplace's method to estimate J. Using $v(y) \sim v_m + v_{yy}(0)y^2/2$ for $y \ll 1$, we get

$$J \sim \sqrt{\frac{2\pi}{c_1^3|v_{yy}(0)|}}e^{c_1 v_m}\,. \tag{5.31}$$

Finally, using (5.22) for v_m and (5.23) for Γ_0, we can estimate the product $\Gamma_0 J$ in (5.30). This leads to the following more explicit result:

Corollary 5.4: *Under the conditions of Proposition 5.3, we have*

$$\frac{dx_0}{dt} \sim \varepsilon^2 \mu \left(\frac{g'(x_0)}{g(x_0)} \right) , \qquad \mu \equiv \frac{v_m}{c_1 \left(\int_{-\infty}^{\infty} [v_y(y)]^2 \, dy \right)} \sqrt{\frac{2\pi}{1 - 2/(c_1 v_m)}} \, . \tag{5.32}$$

Here v_m is given asymptotically in (5.22).

Notice that (5.32) is very similar in form to the corresponding result (4.9b) for the polynomial conductivity model $f(u) = 1 + u^2$. However, the term $\mu > 0$ in (5.32) does depend weakly on x_0. For $g(x)$ as given in (1.2b), (5.32) reduces to

$$\frac{dx_0}{dt} \sim -\frac{\pi \varepsilon^2 \mu \sin(\pi x_0)}{2 \cos^2(\frac{\pi}{2} x_0)} \, . \tag{5.33}$$

Since $\mu > 0$, then $x_0 \to 0$ as $t \to \infty$ for any $x_0(0) \in (-1, 1)$.

The constant μ in (5.33) can be evaluated without requiring pointwise values for the homoclinic orbit $v(y)$. In analogy with (5.11d), we obtain

$$\int_{-\infty}^{\infty} [v_y(y)]^2 \, dy = 2 \int_{\sigma}^{v_m} [-2Q(v)]^{1/2} \, dv \, , \qquad Q(v) \equiv \int_{\sigma}^{v} q(\eta) \, d\eta \, , \tag{5.34}$$

where $q(\eta) \equiv -2\eta + \Gamma_0 g(x_0) e^{c_1 \eta}$. Using our formulae for v_m, Γ_0, and σ, in (5.22), (5.23), and (5.24), respectively, we can then use (5.34) to calculate μ in (5.33). For the realistic parameter values $p_c = 0.66$, $\chi = 0.01$, $c_1 = 1.5$, and for the $g(x)$ of (1.2b), in Fig. 15 we plot μ as a function of x_0 for three values of ε.

Finally, we give a detailed comparison of the asymptotic result (5.33) with full numerical results computed from (1.2) using the NAG library routine D03PCF [22]. In each case below, the parameter values were $p_c = 0.66$, $\chi = 0.01$, $c_1 = 1.5$, with $g(x) = \cos^2(\pi x/2)$. In addition, the initial condition for (1.2) was taken to be

$$u(x, 0) = v_m \mathrm{sech}^2 \left(\frac{\varepsilon^{-1} [x - x_0(0)]}{\sqrt{2}} \right) , \qquad x_0(0) = -0.4 \, . \tag{5.35}$$

Here v_m is given in (5.22) with $x_0(0) = -0.4$. Notice that this initial condition does not have the same profile as the homoclinic orbit for (5.20). Therefore, we expect an initial transient period where the correct hot-spot profile forms from this initial data. For $\varepsilon = 0.1$, in Fig. 16(a) we compare asymptotic and numerical results for the maximum height v_m of the hot-spot as a function of x_0. The asymptotic and numerical results for v_m agree to within 4%. In Fig. 16(b) we show a very favorable comparison between the asymptotic and numerical results for the hot-spot trajectory.

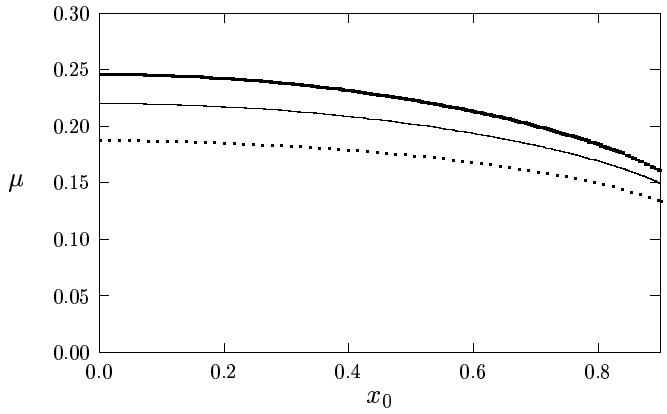

Figure 15: Plots of μ, defined in (5.32), versus x_0 for $\varepsilon = 0.3$ (heavy solid curve), $\varepsilon = 0.2$ (solid curve), and $\varepsilon = 0.1$ (dashed curve). The parameter values are $p_c = 0.66$, $\chi = 0.01$, and $c_1 = 1.5$.

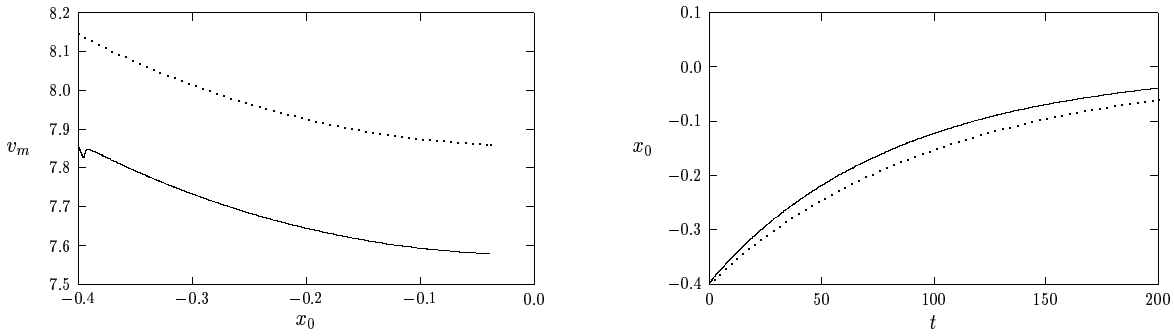

(a) v_m versus x_0

(b) x_0 versus t

Figure 16: The asymptotic results (5.22) for v_m versus x_0, and (5.33) for x_0 versus t, are compared with full numerical results from (1.2). The dashed curves are the asymptotic results, and the solid curves the numerical results. The parameter values are $p_c = 0.66$, $\chi = 0.01$, $c_1 = 1.5$, and $\varepsilon = 0.1$.

By comparing this figure with Fig. 13(a) we observe that the hot-spot evolution is slower for the exponential conductivity model, at these realistic parameter values, than for the polynomial conductivity model. In Fig. 17(a) and Fig. 17(b) we plot the numerically computed solution to (1.2) at different times showing both the initial transient period and the slow approach to an equilibrium hot-spot solution centered at the maximum point of $g(x)$. We remark that the asymptotic result (5.33) for $x_0(t)$ compares very well with corresponding full numerical results at even larger values of ε. In Fig. 18(a) and Fig. 18(b) we compare the asymptotic and numerical hot-spot trajectories when $\varepsilon = 0.2$ and $\varepsilon = 0.3$, respectively. For these two values of ε, in Fig. 19 we plot the numerical solution to (1.2) at a value of t where they are close to the equilibrium solution.

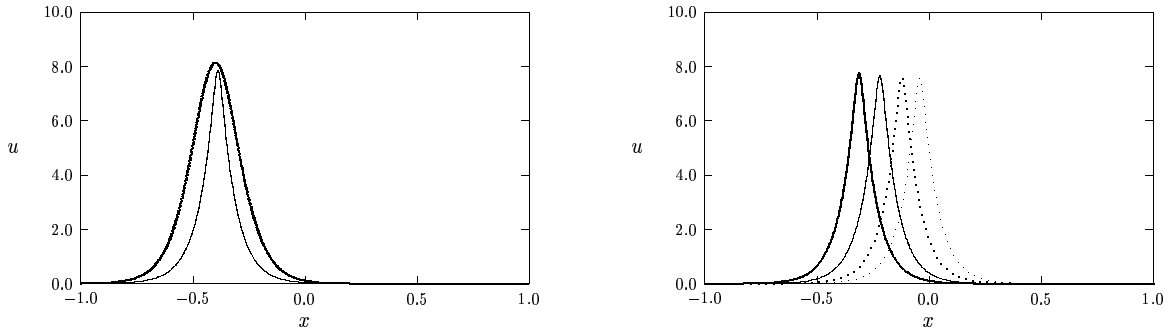

(a) transient period

(b) slow evolution

Figure 17: The numerical solution u to (1.2) at different times. In the left figure, $t = 0$ (heavy solid curve) and $t = 2$ (solid curve). In the right figure, $t = 20.2$ (heavy solid), $t = 50$ (solid), $t = 100$ (dashed), and $t = 195$ (dots). The parameter values are $p_c = 1.0$, $\chi = 0.01$, $c_1 = 1.5$, and $\varepsilon = 0.1$.

6 Discussion

In this paper, we have extended the analysis of [6], [4], [5], [17], and [18], on the stability and dynamics of hot-spot solutions for the microwave heating models (1.1) and (1.2). We have given a new method for proving the stability of hot-spot solutions whenever the linearized operator is not self-adjoint. In the limit $\varepsilon \to 0$, and when the linearized operator around a localized hot-spot solution is not self-adjoint, we have argued that complex conjugate eigenvalues in the unstable

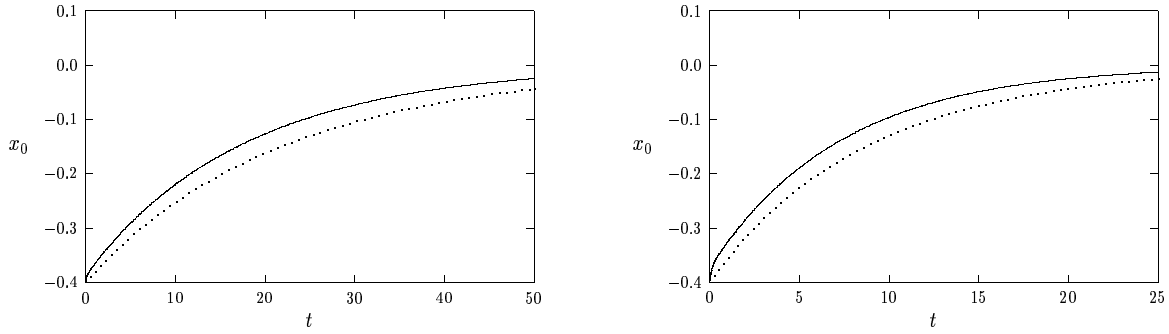

(a) x_0 versus t: $\varepsilon = 0.2$

(b) x_0 versus t: $\varepsilon = 0.3$

Figure 18: Comparison of asymptotic (dashed curves) and full numerical (solid curves) hot-spot trajectories for two values of ε when $p_c = 1.0$, $\chi = 0.01$, and $c_1 = 1.5$.

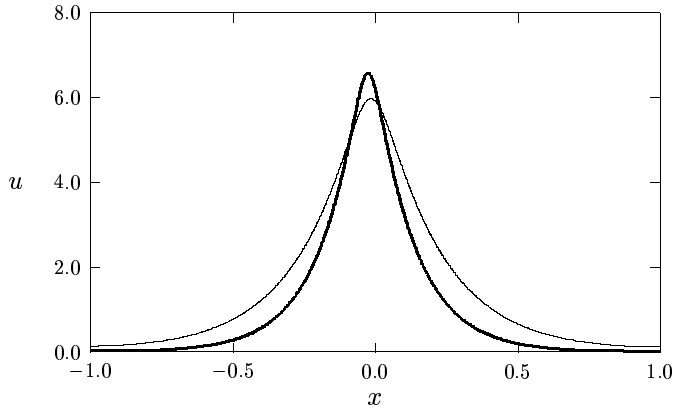

Figure 19: Plots of the numerical solution to (1.2) for $\varepsilon = 0.2$ with $t = 50.0$ (heavy solid curve), and for $\varepsilon = 0.3$ with $t = 24.0$ (solid curve). The parameter values are $p_c = 1.0$, $\chi = 0.01$, and $c_1 = 1.5$. These solutions are very close to the stable equilibrium solution.

right-half plane cannot be excluded from any symmetry considerations, as was done in [6] and [5]. When $\varepsilon \ll 1$, a careful search to rule out such eigenvalues is still required.

We then extended the analysis of [4] and [6] to give an explicit characterization of the dynamics of a metastable hot-spot solution for (1.1) in the limit $\varepsilon \to 0$ when $b = 0$. A formal asymptotic analysis was given to derive a differential equation for the location of the hot-spot. For the polynomial conductivity model $f(u) = 1+u^2$, the asymptotic results for the dynamics were compared favorably with corresponding full numerical results. When $b = 0$, we also extended the analysis of [6] and [5] to derive a differential equation for the motion of a hot-spot for (1.2). The hot-spot was found to be pinned to the location of the maximum of $g(x)$ in (1.2b) as $t \to \infty$. For both conductivity models, we compared the asymptotic results for the hot-spot motion with corresponding full numerical results.

We remark that similar results can be obtained when radiative cooling effects are included. This implies that $b > 0$ in (1.1) and (1.2). Our analysis of the polynomial model $f(u) = 1 + u^2$ in §3 and §4 required that $b \ll \varepsilon^2$. In §5 we required that $b \ll 1$ for the exponential conductivity model. Thus, the polynomial model is more sensitive to b. This conclusion was also observed in [5] and [6]. The general effect of b on (1.1) is to increase the decay rate of the homoclinic solution representing the hot-spot profile. Therefore, the metastable motion is slower when $b > 0$ than when $b = 0$. However, with the typical value $b = 0.01$ (cf. [17], [18]), we expect that the effect of radiative cooling on the hot-spot behavior associated with the exponential conductivity model to not be very significant.

Finally, we remark that it would be interesting to analyze the existence, stability, and dynamics, of locally radially symmetric hot-spot solutions for the extension of (1.1) and (1.2) to two space dimensions. In [18], a hot-spot for a microwave heated slab, modeled by the multi-dimensional extension of (1.2), was computed numerically. Similar localized solutions for the two-dimensional Gierer-Meinhardt model, in the presence of spatially inhomogeneous terms in the differential operator, have been analyzed and computed numerically in [26]. In [18] and [5], a hot-stripe solution for the two-dimensional version of (1.2) was shown analytically to be unstable. The resulting instability was shown numerically to lead to a radially symmetric hot-spot solution located at the center of the slab. This type of instability is very similar in form to the instability that occurs for a stripe solution to the Gierer-Meinhardt model in a two-dimensional domain (cf. [11]). In [11] it was shown that a stripe can be stabilized only when the two-dimensional domain is sufficiently thin. It would be of interest to study these multi-dimensional extensions of (1.1) and (1.2) analytically.

Acknowledgements

D. I. thanks NSERC for their support by way of an NSERC Postdoctoral Fellowship. M. J. W. thanks NSERC and the IMS of the Chinese University of Hong Kong for hosting a period of his sabbatical leave from UBC. We thank Prof. Juncheng Wei of the CUHK for a helpful discussion on the material in §2. We thank the referees for their detailed comments on the original manuscript.

A The Proof of Proposition 2.4

The proof of Proposition 2.4 was given in Propositions 3.1 and 3.2 of [23]. For the convenience of the reader, we outline the key steps here. The proof of Proposition 2.4 relies heavily on two explicit formulae for the local operator L_0 defined in (2.13). By a direct computation, we have

$$L_0^{-1} w_0^p = \frac{w_0}{p-1}\,; \qquad L_0^{-1} w_0 = \frac{w_0}{p-1} + \frac{1}{2} y\, w_0^{'}\,, \tag{A.1}$$

where w_0 is defined in (2.14). Integrating the expression for $\tilde{f}_R$ in (2.27b) by parts, we use (A.1) for $L_0 w_0$, to get

$$\tilde{f}_R(\lambda_I) = (p-1)\frac{\int_{-\infty}^{\infty} w_0^p \left[L_0^2 + \lambda_I^2\right]^{-1} w_0^p\, dy}{\int_{-\infty}^{\infty} w_0^2\, dy}\,. \tag{A.2}$$

Differentiating (A.2) with respect to λ_I, and integrating the resulting expression by parts, we obtain

$$\tilde{f}_R^{'}(\lambda_I) = -2(p-1)\lambda_I \frac{\int_{-\infty}^{\infty} \left(\left[L_0^2 + \lambda_I^2\right]^{-1} w_0^p\right)^2 dy}{\int_{-\infty}^{\infty} w_0^2\, dy} < 0\,. \tag{A.3}$$

This proves (2.28d). The global result (2.28e) for $\tilde{f}_I$ is more difficult to prove (see Proposition 3.2 of [23]). However, this result is not crucial for our analysis.

The asymptotic behavior for $\tilde{f}_R$ and $\tilde{f}_I$ as $\lambda_I \to \infty$ in (2.28a) and (2.28b) is immediately clear. It remains to prove the local behavior for $\tilde{f}_R$ and $\tilde{f}_I$ as $\lambda_I \to 0$ given in (2.28a) and (2.28b). It is clear that all the odd derivatives of $\tilde{f}_R$ at $\lambda_I = 0$ are zero. Using (2.27b) for $\tilde{f}_R$, we calculate that

$$\tilde{f}_R(0) = \frac{\int_{-\infty}^{\infty} w_0 L_0^{-1} w_0^p\, dy}{\int_{-\infty}^{\infty} w_0^2\, dy}\,, \qquad \kappa_c = -\frac{\tilde{f}_R^{''}(0)}{2} = \frac{\int_{-\infty}^{\infty} w_0 L_0^{-3} w_0^p\, dy}{\int_{-\infty}^{\infty} w_0^2\, dy}\,. \tag{A.4}$$

Using (A.1) for $L_0^{-1} w_0^p$, we obtain $\tilde{f}_R(0) = 1/(p-1)$. Next, using (A.1) for $L_0^{-1} w_0^p$, we readily obtain (2.28c) for κ_c. Finally, to establish the local behavior (2.28b) for $\tilde{f}_I$ as $\lambda_I \to 0$, we use

(2.27b) for $\tilde{f}_I$, and (A.1), to get

$$\tilde{f}_I'(0) = \frac{\int_{-\infty}^{\infty} w_0 L_0^{-2} w_0^p \, dy}{\int_{-\infty}^{\infty} w_0^2 \, dy} = \frac{1}{(p-1)} \frac{\int_{-\infty}^{\infty} w_0 L_0^{-1} w_0 \, dy}{\int_{-\infty}^{\infty} w_0^2 \, dy} = \frac{1}{(p-1)} \frac{\int_{-\infty}^{\infty} w_0 \left[\frac{w_0}{p-1} + \frac{1}{2} y w_0' \right] \, dy}{\int_{-\infty}^{\infty} w_0^2 \, dy} . \quad \text{(A.5)}$$

The last integral in (A.5) is readily evaluated upon integrating by parts to obtain (2.28b).

B The Proof of Proposition 2.6

The proof of Proposition 2.6 was given in Proposition 3.5 of [23]. We outline the key steps here. We first derive the local behavior (2.33a) as $\lambda_R \to 0$. From (2.32), we calculate

$$f_R(0) = \frac{\int_{-\infty}^{\infty} w_0 L_0^{-1} w_0^p \, dy}{\int_{-\infty}^{\infty} w_0^2 \, dy} , \quad f_R'(0) = \frac{\int_{-\infty}^{\infty} w_0 L_0^{-2} w_0^p \, dy}{\int_{-\infty}^{\infty} w_0^2 \, dy} , \quad f_R''(0) = \frac{2 \int_{-\infty}^{\infty} w_0 L_0^{-3} w_0^p \, dy}{\int_{-\infty}^{\infty} w_0^2 \, dy} . \quad \text{(B.1)}$$

Using (A.1) for $L_0^{-1} w_0^p$, we get $f_R(0) = 1/(p-1)$. The integral for $f_R'(0)$ was calculated in (A.5). Using (A.1) for $L_0^{-1} w_0^p$, we observe that $f_R''(0) = 2\kappa_c$, where κ_c was defined in (2.28c). This shows (2.33a).

To establish the global result (2.33b), we write $f_R(\lambda_R)$ in (2.32) as

$$f_R(\lambda_R) = \frac{\int_{-\infty}^{\infty} w_0 \left(L_0 - \lambda_R \right)^{-1} \left[\left(L_0 - \lambda_R \right) w_0 + \lambda_R w_0 \right] \, dy}{(p-1) \int_{-\infty}^{\infty} w_0^2 \, dy} = \frac{1}{(p-1)} + \frac{\lambda_R \int_{-\infty}^{\infty} w_0 \left(L_0 - \lambda_R \right)^{-1} w_0 \, dy}{(p-1) \int_{-\infty}^{\infty} w_0^2 \, dy} . \quad \text{(B.2)}$$

By differentiating (B.2) we obtain

$$f_R'(\lambda_R) = \frac{1}{(p-1)} \frac{\int_{-\infty}^{\infty} w_0 \left(L_0 - \lambda_R \right)^{-1} w_0 \, dy}{\int_{-\infty}^{\infty} w_0^2 \, dy} + \frac{\lambda_R}{(p-1)} \frac{\int_{-\infty}^{\infty} \left[\left(L_0 - \lambda_R \right)^{-1} w_0 \right]^2 \, dy}{\int_{-\infty}^{\infty} w_0^2 \, dy} . \quad \text{(B.3)}$$

We define the auxiliary functions $h_1(\alpha)$ by

$$h_1(\alpha) = \int_{-\infty}^{\infty} w_0 \left(L_0 - \alpha \right)^{-1} w_0 \, dy . \quad \text{(B.4)}$$

From (B.3), the result $f_R'(\lambda_R) > 0$ follows if we can show that $h_1(\alpha) \geq 0$ on $0 \leq \alpha < \nu_0$. Here $\nu_0 > 0$ is the principal eigenvalue of the local operator L_0. From differentiating $h_1(\alpha)$ in (B.4), it is clear that $h_1'(\alpha) > 0$. Next, we use (B.4) and (A.1) to calculate

$$h_1(0) = \int_{-\infty}^{\infty} w_0 L_0^{-1} w_0 \, dy = \int_{-\infty}^{\infty} \left(\frac{w_0^2}{p-1} + \frac{1}{2} y w_0 w_0' \right) \, dy = \left(\frac{1}{p-1} - \frac{1}{4} \right) \int_{-\infty}^{\infty} w_0^2 \, dy . \quad \text{(B.5)}$$

Thus, when $1 < p \le 5$ we have $h_1(0) \ge 0$. Since $h_1'(\alpha) > 0$, we obtain that $h_1(\alpha) > 0$ on $0 < \alpha < \nu_0$. Thus, $f_R' > 0$ on $(0, \nu_0)$ when $1 < p \le 5$. This proves (2.33b). The proof of (2.33c) is a consequence of Lemma 3.6 of [23] that proves that when $\lambda_R > \nu_0$, the solution ξ to $(L_0 - \lambda_R)\,\xi = v$ satisfies $\xi < 0$ on $-\infty < y < \infty$ whenever $v > 0$ on $-\infty < y < \infty$.

C Nonlocal Eigenvalues and the Gierer-Meinhardt Model

In a one-dimensional domain, and in the limit of an asymptotically large inhibitor diffusivity, the Gierer-Meinhardt activator-inhibitor model reduces to a scalar nonlocal partial differential equation of the form (see [14]):

$$a_t = \epsilon^2 a_{xx} - a + \frac{a^p}{h^q}, \qquad -1 < x < 1\,, \quad t > 0\,, \tag{C.1a}$$

$$h = \left(\frac{1}{2\varepsilon}\int_{-1}^{1} a^m\,dx\right)^{\frac{1}{s+1}}\,, \qquad a_x(\pm 1, t) = 0\,. \tag{C.1b}$$

Here $\varepsilon \ll 1$, $a(x,t)$ and $h(t)$ are the activator and inhibitor concentrations, and the exponents satisfy

$$p > 1\,, \qquad q > 0\,, \qquad m > 0\,, \qquad s \ge 0\,. \tag{C.1c}$$

A one-spike equilibrium solution to (C.1), with the spike centered at the midpoint $x = 0$ of the domain, has the form

$$a_e \sim h_e^{q/(p-1)} w_\varepsilon\left(x/\varepsilon\right)\,, \qquad h_e \sim \left(\frac{1}{2}\int_{-1/\varepsilon}^{1/\varepsilon} [w_\varepsilon(y)]^m\,dy\right)^{\frac{p-1}{(s+1)(p-1)-qm}}\,. \tag{C.2}$$

Here $w_\varepsilon(y)$ is the one-pulse solution satisfying (2.12). To determine the stability of this solution, we let

$$a(x,t) = a_e(x) + e^{\lambda^\varepsilon t}\Phi^\varepsilon\left(x/\varepsilon\right)\,, \qquad h(t) = h_e + e^{\lambda^\varepsilon t}\eta\,. \tag{C.3}$$

Substituting (C.3) into (C.1), and linearizing in the usual way, we obtain the following nonlocal eigenvalue problem for $\Phi^\varepsilon(y)$:

$$\Phi^\varepsilon_{yy} + \left(-1 + p w_\varepsilon^{p-1}\right)\Phi^\varepsilon - \alpha w_\varepsilon^p\left(\frac{\int_{-1/\varepsilon}^{1/\varepsilon} w_\varepsilon^{m-1}\Phi^\varepsilon\,dy}{\int_{-1/\varepsilon}^{1/\varepsilon} w_\varepsilon^m\,dy}\right) = \lambda^\varepsilon\Phi^\varepsilon\,, \qquad |y| \le 1/\varepsilon\,, \tag{C.4a}$$

$$\Phi^\varepsilon_y(\pm\varepsilon^{-1}) = 0\,. \tag{C.4b}$$

Here α is the positive constant

$$\alpha \equiv \frac{mq}{s+1}\,. \tag{C.4c}$$

We note that (C.4) has precisely the same form as given in (2.10). The problem (C.4) with $\alpha = 2p$ and $m = p$ also arises in the study of the stability of hot-spot solutions for the polynomial conductivity model $f(u) = 1 + c_1 u^p$ (see §3.4). For the Gierer-Meinhardt model it is usually assumed that, in addition to (C.1c), the exponents (p, q, m, s) of the nonlinearities in (C.1) satisfy $qm/(s+1) > (p-1)$, which translates to $\alpha > (p-1)$. In §2.2 and §2.3 we do not impose this restriction on α, and instead study (C.4) for any value of $\alpha \geq 0$.

References

[1] E. Anderson et al. *Lapack User's Guide: Third Edition*, SIAM Publications (1999).

[2] U. Ascher, R. Christiansen, R. Russell, *Collocation Software for Boundary Value ODE's*, Math. Comp., **33**, (1979), pp. 659-679.

[3] M. Booty, G. Kriegsmann, *Microwave Heating and Joining of Ceramic Cylinders: A Mathematical Model*, Meth. Appl. Anal., **4**, No. 1, (1994), pp. 403-414.

[4] A. Bose, G. Kriegsmann, *Stability of Localized Structures in NonLocal Reaction-Diffusion Equations*, Meth. Appl. Anal., **5**, No. 4, (1998), pp. 351-366.

[5] A. Bose, G. Kriegsmann, *Large Amplitude Solutions of Spatially Non-Homogeneous NonLocal Reaction-Diffusion Equations*, Meth. Appl. Anal., **7**, No. 2, (2000), pp. 295-311.

[6] A. Bose, *A Geometric Approach to Singularly Perturbed Nonlocal Reaction Diffusion Equations*, SIAM J. Math. Anal., **31**, No. 2, (2000), pp. 431-454.

[7] S.J. Chapman, G. Richardson, *Vortex Pinning by Inhomogeneities in Type-2 Superconductors*, Physica D, **108**, (1997), pp. 397-407.

[8] P. De Groen, G. Karadzhov, *Metastability in the Shadow System for Gierer-Meinhardt's Equations*, Electronic Journal of Differential Equations, No. 50, (2002), pp.1-22.

[9] A. Doelman, R. A. Gardner, T. Kaper, *Large Stable Pulse Solutions in Reaction-Diffusion Equations*, Indiana U. Math. Journ., **50**, No. 1, (2001), pp. 443-507.

[10] A. Doelman, T. J. Kaper, P. Zegeling, *Pattern Formation in the One-Dimensional Gray-Scott Model*, Nonlinearity, **10**, (1997), pp. 523-563.

[11] A. Doelman, H. van der Ploeg, *Homoclinic Stripe Patterns*, SIAM J. Appl. Dyn. Systems, **1**, No. 1, (2002), pp. 65-104.

[12] P. Freitas, *A Nonlocal Sturm-Liouville Eigenvalue Problem*, Proc. Roy. Soc. Edin., **124A**, (1994), pp. 169-188.

[13] P. Freitas, G. Sweers, *Positivity Results for a Nonlocal Elliptic Equation*, Proc. Roy. Soc. Edinburgh, Vol. 128A, (1998), pp. 697-715.

[14] D. Iron, M. J. Ward, *A Metastable Spike Solution for a Nonlocal Reaction-Diffusion Model*, SIAM J. Appl. Math., **60**, No. 3, (2000), pp. 778-802.

[15] D. Iron, M. J. Ward, J. Wei, *The Stability of Spike Solutions to the One-Dimensional Gierer-Meinhardt Model*, Physica D, **150**, No. 1-2, (2001), pp. 25-62.

[16] D. Iron, M. J. Ward, *Spike Pinning for the Gierer-Meinhardt Model. Nonlinear Waves: Computation and Theory (Athens, GA, 1999)*, Math. Comput. Simul., **55**, No. 4-6, (2001), pp. 419-431.

[17] G. Kriegsmann, *Hot Spot Formation in Microwave Heated Ceramic Fibers*, IMA J. Appl. Math., **52**, (1997), pp. 123-148.

[18] G. Kriegsmann, *Pattern Formation in Microwave Heated Ceramics: Cylinders and Slabs*, IMA J. Appl. Math., **66**, No. 1, (2001), pp. 1-32.

[19] A. A. Lacey, *Thermal Runaway in a NonLocal Problem Modeling Ohmic Heating: Part 1: Model Derivation and Some Special Cases*, Europ. J. Appl. Math., Vol. **6**, (1995), pp. 127-144.

[20] F. H. Lin, Q. Du, *Ginzburg-Landau Vortices: Dynamics, Pinning and Hysteresis*, SIAM J. Math. Anal., **28**, (1997), pp. 1265-1293.

[21] C. S. Lin, W. M. Ni, I. Takagi, *Large Amplitude Stationary Solutions to a Chemotaxis System*, J. Diff. Eq., **72**, (1988), pp. 1-27.

[22] NAG Fortran library Mark 17, routine D03PCF, Numerical Algorithms Group Ltd., Oxford, United Kingdom (1995).

[23] M. J. Ward, J. Wei, *Hopf Bifurcation and Oscillatory Instabilities of Spike Solutions for the One-Dimensional Gierer-Meinhardt Model*, J. Nonlinear Science, March (2003), electronic, (58 pages).

[24] M. J. Ward, *Eliminating Indeterminacy in Singularly Perturbed Boundary Values Problems with Translation Invariant Potentials*, Stud. Appl. Math., **87**, (1992), pp. 95-135.

[25] M. J. Ward, *Exponential Asymptotics and Convection-Diffusion-Reaction Models*, book chapter in *Analyzing Multiscale Phenomena Using Singular Perturbation Methods*, (J. Cronin, R. O'Malley editors), Proceedings of Symposia in Applied Mathematics, Vol. 56, AMS Short Course (1998), pp. 151-184.

[26] M. J. Ward, D. McInerney, P. Houston, D. Gavaghan, P. Maini, *The Dynamics and Pinning of a Spike for a Reaction-Diffusion System*, SIAM J. Appl. Math., **62**, No. 4, (2002), pp. 1297-1328.

[27] J. Wei, *On Single Interior Spike Solutions for the Gierer-Meinhardt System: Uniqueness and Stability Estimates*, Europ. J. Appl. Math., Vol. **10**, No. 4, (1999), pp. 353-378.

[28] J. Wei, M. Winter, *A Nonlocal Eigenvalue Problem and the Stability of Spikes for Reaction-Diffusion Systems with Fractional Reaction Rates*, Int. Journ. Bifur. and Chaos, to appear, (2003).